Journal of Environmental Chemical Engineering 13 (2025) 115499

Contents lists available at ScienceDirect

Journal of Environmental Chemical Engineering

journal homepage: www.elsevier.com/locate/jece

Converting rice husk biomass into value-added materials for low-carbon economies: Current progress and prospect toward more sustainable practices

Ngoc N. Nguyen *, Anh V. Nguyen, Muxina Konarova

School of Chemical Engineering, The University of Queensland, Brisbane, QLD 4072, Australia

ARTICLE INFO

Keywords:
Biomass conversion
Circular economy
Waste recycling
Energy materials
Rice husk
Agrowaste
Hydrogen generation

ABSTRACT

The abundant rice husk agrowaste possesses a silicon-rich composition in the form of natural biogenic silicon/carbon blend. This unique property of rice husk (RH) enables the preparation of nanohybrid materials with particular properties which are otherwise difficult to achieve via synthetic means. RH-derived nanostructured materials show promising applications in low-carbon economies such as heterogeneous catalysts for hydrogen generation and decarbonisation, battery anodes, supercapacitors, drug carriers, quantum dots, solar grade silicon, and adsorbents. Here, we discuss the latest advances in converting RH into such value-added materials and highlight the drawbacks of the current methods which are unsustainable due to high consumptions of energy and harsh chemicals. We elaborate a distinctive forward-looking perspective on the transition toward more sustainable practices via enzymatic processing, microwave- or ultrasound-assisted conversion, and the use of eco-friendly chemicals, for more energy- and cost-efficient productions of RH-derived products. Insights provided by this paper promote the progress in agrowaste recycling toward a circular decarbonised world.

1. Introduction

Repurposing biomass towards value-added commodities plays an integral role in the circular low-carbon economy [1,2]. It allows us to achieve the dual purpose considering the environmental and economic benefits [2]. Among agrowastes, rice husk (RH) has attracted a significant research interest due to its abundance and its high silicon content, presenting unique opportunity for the development of nanostructured silica materials [3].

The global capacity of rice production currently reaches 500 million metric tons per year and continues to increase steadily in the future following the growth of the world population [4]. Every kilogram of milled rice entails ~ 0.28 kg of RH as a by-product of the rice milling process, i.e., rice husk accounts for about 25 % of the weight of the rice paddy grain [5,6]. This leads to the annual generation of 140 million metric tonnes of RH as agrowaste. The composition of RH shows somewhat dependence on geographical regions, yet it typically contains cellulose (~50 wt%), lignin (25–30 wt%), ash (15–20 wt%) and moisture (10–15 wt%) [7]. Importantly, the main component of rice husk ash (RHA) is SiO_2, accounting for 80–90 wt% of the ash [8]. The balance is constituted by other metal oxides such as K_2O, Na_2O, CaO, MgO, Al_2O_3, etc. [8].

Hence, RH is rich in both carbon and silicon - two pivotal elements in advanced material engineering [3]. Although both carbon and silicon are abundant on Earth, the fossil-derived carbon (e.g., coal) and silicon (e.g., quartz) are less reactive and require harsh conditions for processing, entailing significant costs and environmental footprints [2]. In contrast, the biogenic carbon and silicon in RH are highly reactive and naturally blended at molecular levels (organometallic complexes), and present a starting point for the synthesis of nanostructured functional materials with minimal economic and environmental costs. It is highly feasible to separate the carbonaceous components from the silicon counterpart to derive both functional carbon materials and amorphous ultrapure silica [9,10]. Alternatively, one can take the advantage of the naturally blended biogenic carbon/silicon to derive nano-composite materials with tailored properties which are otherwise not possible to achieve via synthetic means [11–15]. These nanohybrid materials show potential for applications in cutting-edge areas such as heterogeneous catalysts [16], hydrogen generation [17], environmental remediation [16, 18–20], energy materials, battery anodes [11–15], drug carriers [21], supercapacitors [22], ultrapure silicon (solar grade silicon) [23], quantum dots [24], etc. Complementary to these emerging directions

* Corresponding author.
E-mail address: n.nguyen9@uq.edu.au (N.N. Nguyen).

https://doi.org/10.1016/j.jece.2025.115499
Received 26 November 2024; Received in revised form 14 January 2025; Accepted 16 January 2025
Available online 17 January 2025

are enduring interests in turning RH into conventional materials such as amorphous silica, adsorbents, fillers, binders and additives for cement and polymers. Owing to these exceptional advantages with respect to the abundant quantity and excellent quality, RH presents a precious resource for the synthesis of advanced functional materials (Fig. 1). Consequently, the research into repurposing RH has thrived over the past decades, with an exponential growth in the number of publications (Fig. 2). Given the significance of this field, there have been a number of well-received topical reviews published in the literature, for example, the references [25–29]. However, those reviews either focused on one type of RH-derived materials (e.g., silica, adsorbents or fillers) or dedicated to specific applications of these materials, whilst the latest advances and emerging directions have not been discussed systematically in the literature, in particular, the potential applications of RH-derived materials in the energy transition and decarbonisation sectors. Our present review offers a comprehensive overview with in-depth discussions about the unique potential of RH-derived materials in emerging sectors of energy transition and decarbonisation. This paper with the comprehensive and critical discussions based on the state-of-the-art literature offers a valuable contribution and provides a nice piece of reference for motivating and navigating the future research into the development of RH-derived nanostructured hybrid materials for the context of a circular economy.

2. Pushing the boundary of biogenic silica extraction

Around 500 million tons of functional silica is traded in 2024 and this figure will increase to 700 million tons in 2029 [30]. The surging demand for functional silica follows its huge consumption in various essential sectors such as building and construction materials, glass manufacturing, chemical synthesis, water treatments, food industry, cosmetics, and material engineering. RH presents an excellent precursor for the production of high-purity amorphous silica owing to the biogenic nature and high reactiveness of the organometallic complexes. Intensive research has been pushing the boundary of biogenic silica extraction from RH by aiming to improve the quality of the nano-structured RH-derived silica (denoted as RH-silica or RH-SiO_2) with desired structures and morphological properties while enhancing the cost- and energy-efficacy of the silica extraction process. Undoubtedly, establishing the capable methods for producing RH-SiO_2 with desired structures and properties is the prerequisite for the development of value-added functional materials based on RH-derivatives. Hence, this section will cover the latest advances in the extraction of RH-SiO_2.

Given the biogenic nature of silicon in RH, it is expected that the production of RH-silica is relatively easier and less energy-intensive compared to metallurgical processes needed for Earth-sourced silica. Generally, the production of RH-silica requires a combination of thermal and chemical processes. The thermal process (decarbonation) is mainly based on open-air calcination for the removal of carbon and other combustible components. The chemical process, on the other hand, is used for the removal of other metal oxides to yield silica products. Examples of the chemical process include selective dissolution of alkalines, leaching of alkalines, selective precipitation of silica from solutions, etc. The thermal and chemical processes can take place in either orders, but the sequence of them can affect the properties of the resulting silica.

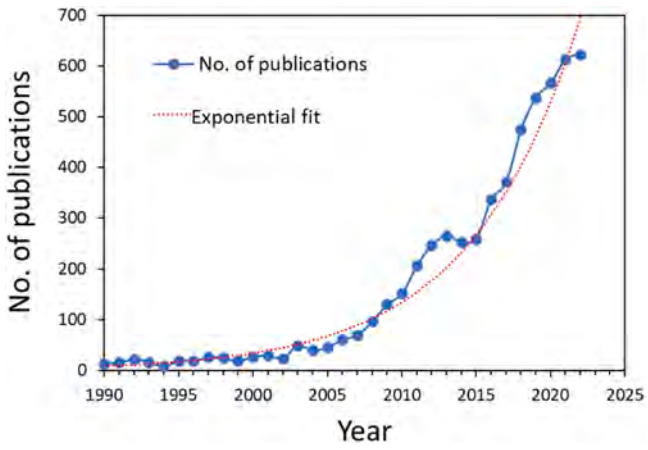

Fig. 2. The exponential growth of literature in repurposing rice husk. Data was obtained from Web of Science by searching articles containing "rice husk" in the titles.

The chemical and structural properties of RH-silica can be tailored by tuning the processing conditions. Researchers have demonstrated the ability to produce RH-silica with varying chemical purity, nanoscale structures, morphology, porosity, specific surface area as well as other material properties such as bandgap and pozzolanic reactivity [9]. The tunable properties of the RH-silica have entailed active research in customised nanostructured silica for various applications. Nguyen et al. investigated and compared two methods for the preparation of RH-silica, called the alkaline-extraction route and the SiO_2-precipitation route (Fig. 3a) [10]. In the alkaline-extraction route, the alkalines in RH were leached in a boiling HCl solution. Then, the alkalines-depleted RH was calcinated at the desired temperature between 500 and 900 °C in an open-air environment for the decarbonation to yield amorphous silica.

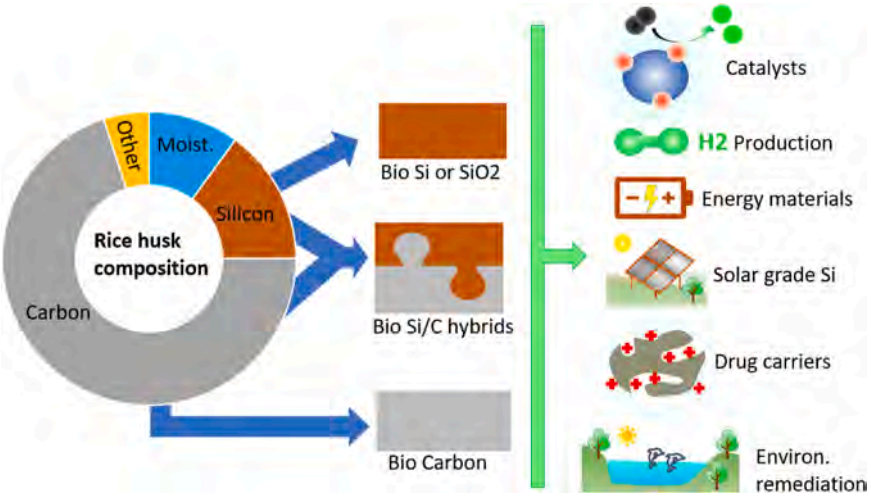

Fig. 1. Featured potential applications of RH-derived nanostructured materials in a circular economy owing to the inherent hybrid nature of naturally blended silicon/carbon in RH. The doughnut-style pie chart represents the composition of raw RH. See text for details.

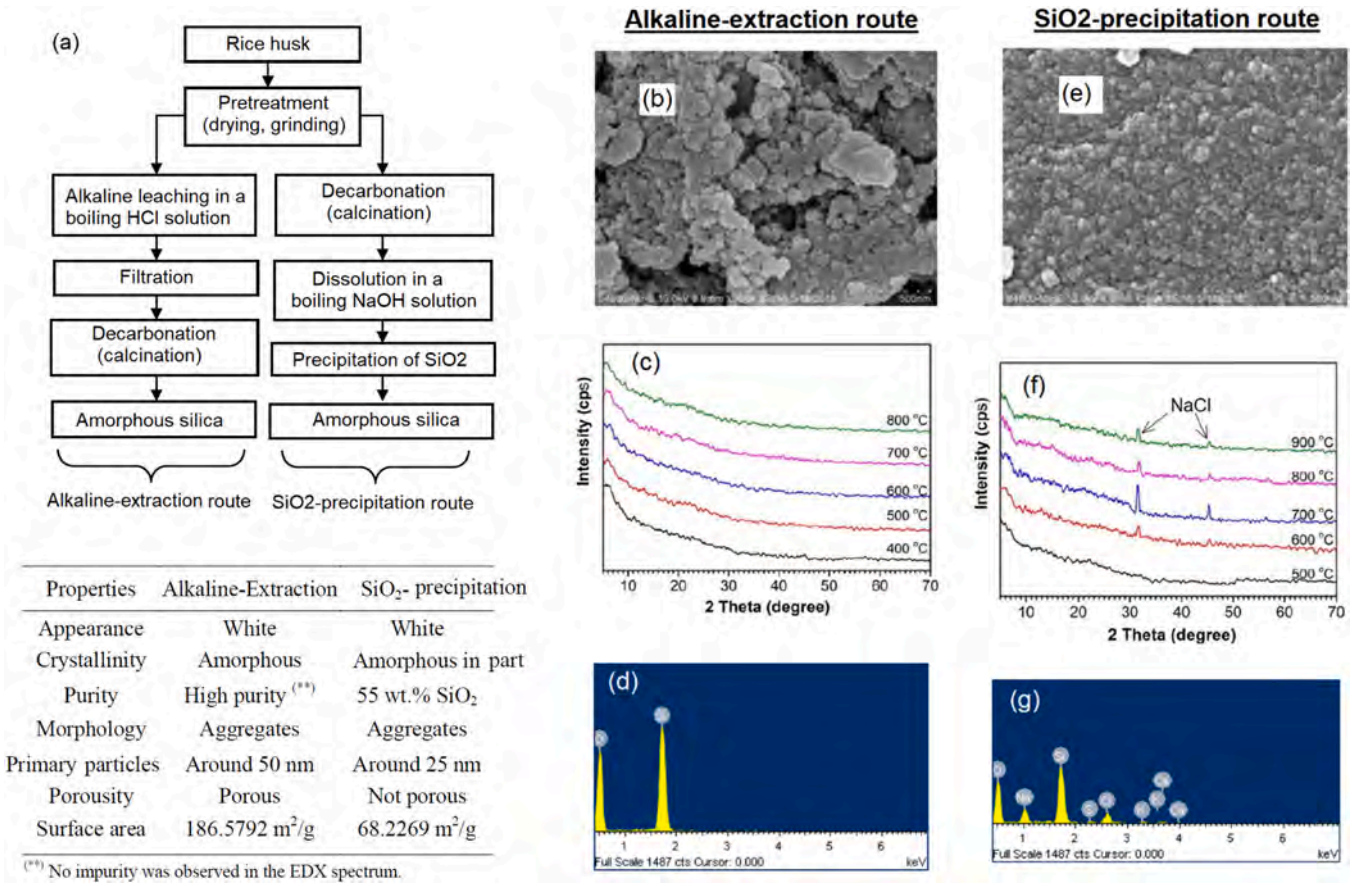

Properties	Alkaline-Extraction	SiO_2- precipitation
Appearance	White	White
Crystallinity	Amorphous	Amorphous in part
Purity	High purity (**)	55 wt.% SiO_2
Morphology	Aggregates	Aggregates
Primary particles	Around 50 nm	Around 25 nm
Porousity	Porous	Not porous
Surface area	186.5792 m^2/g	68.2269 m^2/g

(**) No impurity was observed in the EDX spectrum.

Fig. 3. Ultrapure amorphous RH-derived silica produced using the two methods as indicated (a). The alkaline-extraction yielded an ultrapure amorphous and porous silica as evidenced by the SEM image (b), XRD pattern (c) and EDX spectrum (d). In contrast, the silica obtained from SiO_2-precipitation showed less porosity and evidence of impurities as observed in SEM image (e), XRD pattern (f) and EDX spectrum (g). Figures reproduced with permission from reference [10]. Copyright 2018 Wiley.

In the SiO_2-precipitation route, the RH was first decarbonated through calcination at a desired temperature between 500 and 900 °C to yield a rice husk ash (RHA) which was then dissolved in a boiling NaOH solution, followed by a selective precipitation process to form H_2SiO_3. Afterward, the H_2SiO_3 precipitate was filtered and dried at 110 °C for 3 hours to produce SiO_2 as a silica powder [10]. Nguyen et al. indicated that both methods could produce silica powder with amorphous nature as evidenced by the absence of diffraction peaks in the XRD patterns (Fig. 3). The silica produced via alkaline-extraction was ultrapure as no impurity other than Si and O elements representing SiO_2 was detected from energy-dispersive X-ray spectroscopy - EDX (Fig. 3d). In contrast, the silica produced via SiO_2-precipitation contained significant amounts of crystalline NaCl and other impurities as evidenced by both XRD diffraction pattern and EDX spectrum (Fig. 3f-g)

A large body of research has centered around tuning the synthesis conditions to tailor the properties of RH-silica. Lee et al. used different chemicals (i.e., sulfuric acid, hydrogen chloride, oxalic acid, and 1-butyl-3-methylimidazolium hydrogen sulfate) for removing the metallic compounds from RH to yield silica products [31]. They found that sulfuric acid and 1-butyl-3-methylimidazolium hydrogen sulfate were very efficient chemicals for leaching metallic components and producing silica with high purity, namely 99.6 % and 99.5 %, respectively. In addition, the silica produced using 1-butyl-3-methylimidazolium hydrogen sulfate also showed improved surface area by a factor of 1.9 and pore volume by a factor 2.4 compared to the baseline. Sankar et al. applied a sonochemical method for the production of amorphous spherical silica powder from RH for potential applications as nano-biosensors and energy storage nano-devices [32]. They found that tuning the sonication time provided a feasible way to tailoring properties of the resultant silica such as particle size, porosity and bandgap. Specifically, by increasing the sonication time from 0 to 50 min, the mean particle size augmented from 5 to 40 nm while the bandgap was reduced from 5.77 to 5.68 eV [32]. Dhaneswara et al. successfully obtained high-purity silica from RHA through alkaline extraction (using NaOH solutions at concentrations between 5 % and 10 %) in a reflux process followed by acid treatments with either 1 M hydrochloric acid (HCl) or 1 M acetic acid to yield a silica gel [33]. They showed the superior effect of HCl over acetic acid with respect to the silica properties. The HCl-based process produced silica with a specific surface area of 236 m^2/g and a porosity of 0.54 cc/g, which are higher than the respective values of 204 m^2/g and 0.43 cc/g in the acetic acid-based process [33]. Considering the biocompatibility, Park et al. indicated that RH-derived silica produced via alkali extraction was much more biocompatible than those produced via combustion or acid-leaching processes [34]. Their toxicity tests using human and mouse cells revealed that the dosage causing 50 % loss in viability (LC50) increased in the sequence of combustion-produced silica (LC50 = 500 mg/L), acid-leached silica (LC50 = 500–2000 mg/L) and alkali-extracted silica (LC50 >2000 mg/L) [34].

It is vital to derive silica with desired structures to suit specific applications. This requirement has driven interest in controlling structural properties of RH-silica. Chun et al. reported their success in the synthesis of RH-derived ordered mesoporous silica (OMS) with various topological shapes [35]. The tuning of silica structures was enabled by employing different synthesis routes based on acid leaching, dissolution, and precipitation with the aid of surfactants. The obtained silica showed

various structural conformations ranging from mesocellular forms, to hexagonal nanochannels and irregular spherical or cylindrical aggregates, with a great diversity in the pore size, pore volume and specific surface area (Fig. 4) [35]. Kim et al. reported a method for controlling the size and shape of RH-silica using polyethylene glycol and temperature adjustment during the precipitation step to achieve spherical silica particles with sizes between ~250 nm and ~1.4 μm and a specific surface area over 200 m^2/g [36]. Kordatos et al. reported the synthesis of ZSM-5 zeolite using crystalline RHA as the precursor [37]. RHA was reacted with the organic template TPABr at low temperature and under ambient pressure to produce ZSM-5 with microporous structure and a high surface area of 397 m^2/g [37].

Apart from silica, RH also contains other valuable components such as cellulose and lignin which are precious precursors for producing structured carbon materials. Hence, the simultaneous recovery of multiple components will maximise the value of RH. For example, Jung et al. reported an attempt to recover both the silica and carbon of RH in the forms of nano-structured silica and cellulose nano-fibrils, respectively [38]. Starting from 1000 g of RH, they obtained 119 g of fermentable sugar, 143 g of silica powder (grade >98 %, specific surface area of 328 m^2/g and 273.1 g of functional cellulose nano-fibrils (cellulose > 80.1 %) [38]. Likewise, Nguyen et al. reported a simple biorefining process based on alkaline peroxide leaching coupled with acid precipitation and ethanol extraction to produce different RH-derived products [39]. They achieved bundles of micron-sized fiber-like cellulose and irregular-shaped lignocelluloses products made of > 90 wt% carbon with 52.28 % crystalline fraction [39]. Wei et al. concurrently derived lignocellulose aerogel and amorphous silica nanoparticles from RH [40]. First, RH was dissolved in 1-butyl-3-methylimidazolium chloride, followed by a cyclic liquid nitrogen freeze-thaw process to produce a lignocellulose freeze gel which was then dried by a CO2 supercritical drying process to produce multi-functional self-assembled lignocellulose aerogel [40]. In the meantime, the residue after the lignocellulose extraction was calcined to produce amorphous silica nanoparticles [40]. Featured achievements in RH-SiO_2 production are tabulated in Table 1.

3. RH-derived sustainable battery anodes

Batteries play vital roles in the global roadmap toward sustainable world. Continuing efforts have put on the development of high-performing batteries to boost the energy transition into electrification for carbon-neutral economies. Porous silicon/carbon nanocomposite presents a promising material to overcome the limitation of graphite as an anode material [44]. The inherent silicon/carbon hybrid nature of RH in the form of organometallic compounds provides a unique opportunity for the fabrication of efficient low-cost battery anodes based on silicon carbide hybrids [11–15]. The intrinsic synergy between the RH-derived carbon matrix and silica nanocrystals has been increasingly recognised. Silicon nanocrystals possess low discharge potential and high specific capacity while the carbon matrix has high porosity and good electrical conductivity (Sekar et al. [45]). In addition, the flexibility of RH-derived carbon matrix creates a protective layer to compensate the volumetric variation of Si anode during the repeated lithiation/delithiation process (Ma et al. [46]).

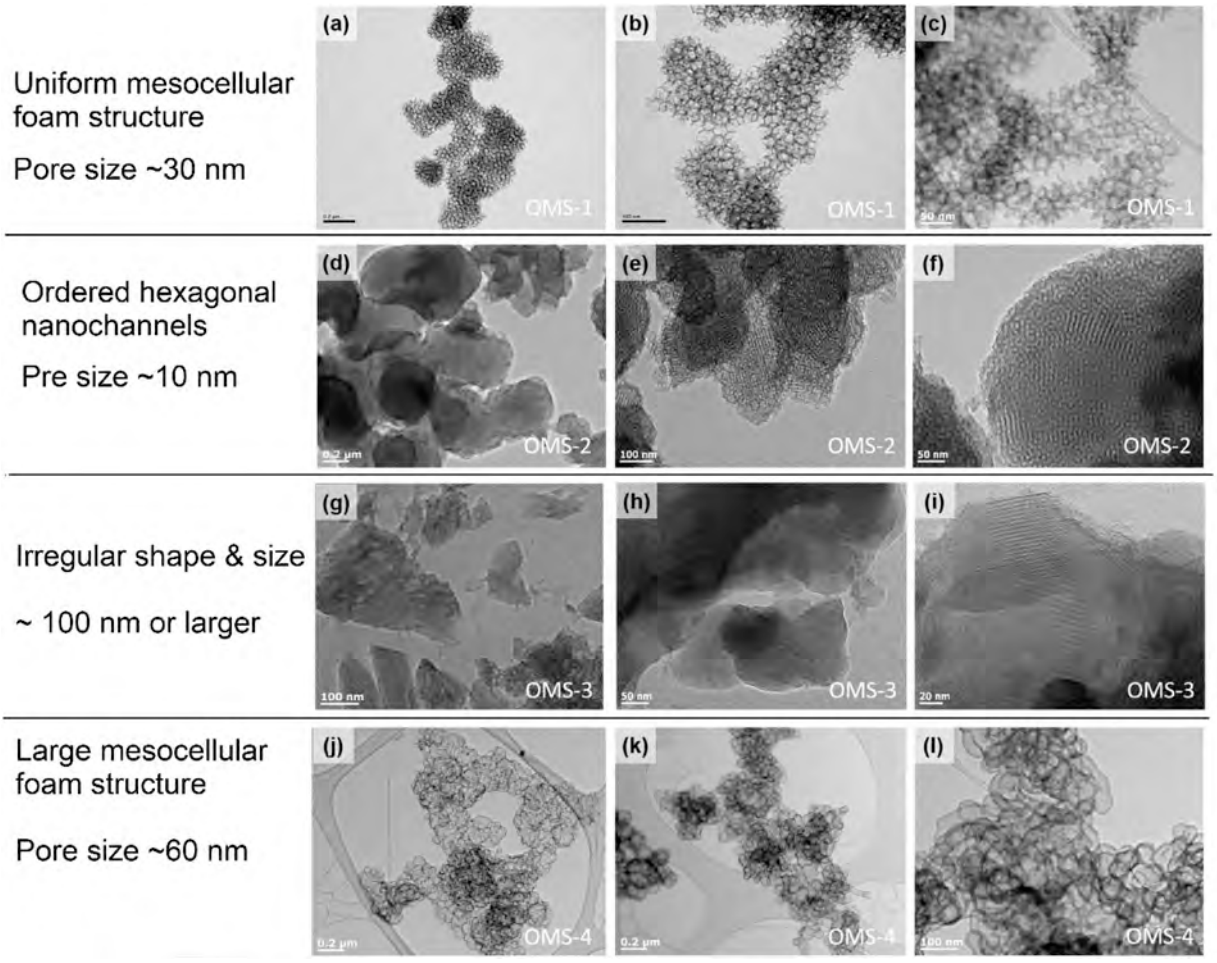

Fig. 4. Different topological shapes of ordered mesoporous silica (OMS) derived from RH. The diversity in structural properties was enabled by tuning the synthesis conditions with the aid of surfactants. Figure reproduced with permission from reference [35], Copyright 2020 Elsevier.

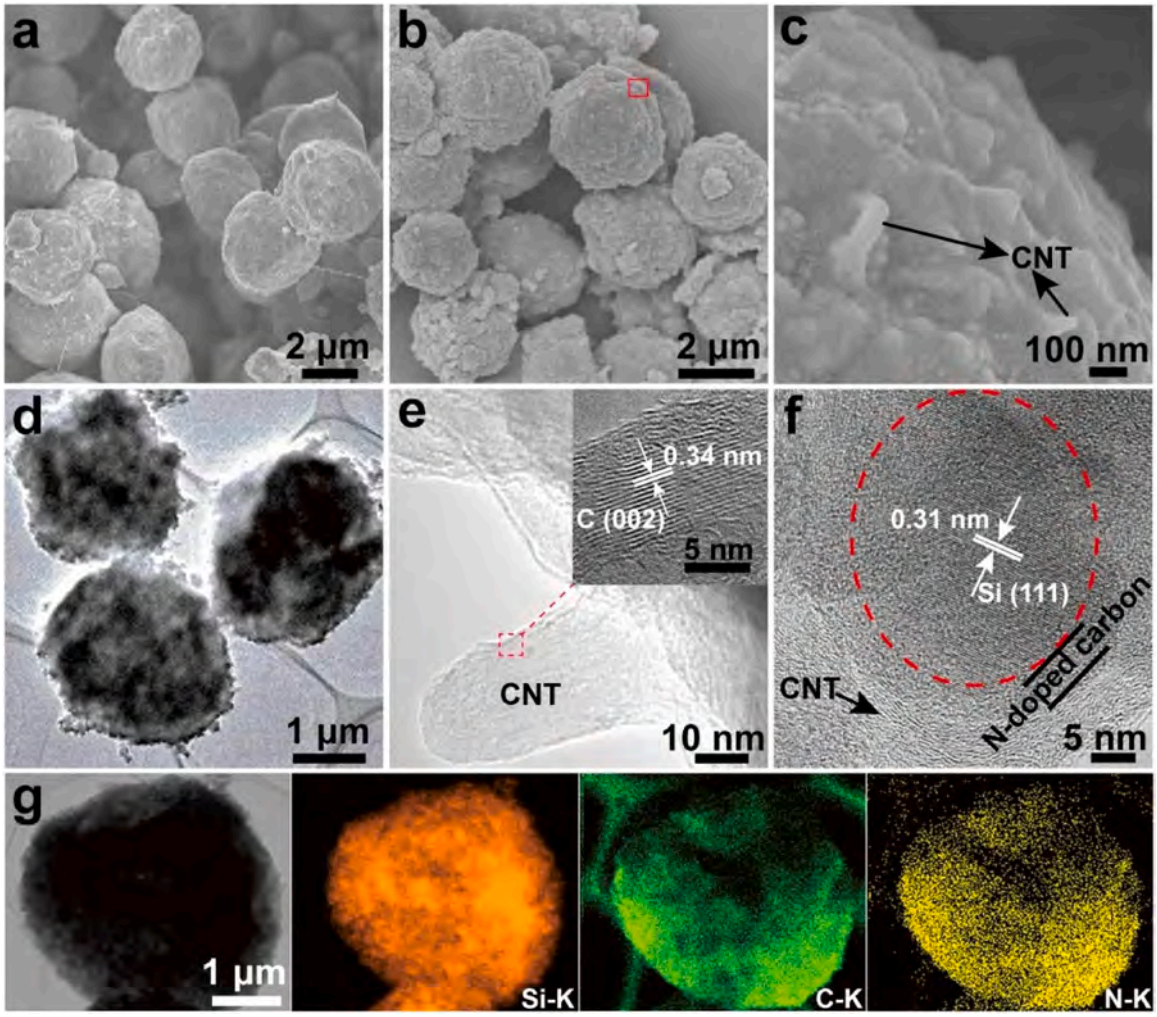

Fig. 5. RH-derived Si/C nanocomposites containing silicon embedded on nitrogen-doped carbon nanotube spheres (Si@N-doped/carbon) for anode materials in Li-ion batteries. SEM images of the precursor prepared via electrospray (a) and the Si@N-doped/carbon (b). A high-magnification SEM image (c) shows a closer look at the marked area in image (b). Typical TEM image (d), high-magnification TEM image (e), high-resolution TEM image (f) and element mapping images (g) of the Si@N-doped/carbon. Reproduced with permission from reference [52]. Copyright 2016 Elsevier.

This exceptional potential has sparked enormous interest in developing anode materials from RH. Gao et al. synthesized nanoporous silicon carbide from RH with a high specific surface area (186.45 m^2/g) via magnesiothermic reduction at 950 °C. They recovered 88.46 % of silicon together with potassium (yield: 91.5 %) and phosphorus (65.5 %) from RH, attesting the substantial potential of producing porous SiC [47]. Li et al. synthesized lignin-SiO_2 composites from RH via carbonisation, ball milling, magnesiothermic reduction and additive treatment [48]. The resulting RH-derived Si/C composite showed stable cycling performance with a high specific capacity retention of 572 mA × h/g at 1.0 A/g after 1000 cycles, which present excellent properties for applications as battery anodes [48]. Lin et al. prepared Si/C nanocomposite via baking the precursor at 400 °C in air followed by reduction in molten $AlCl_3$, yielding to crystalline Si nanoparticles supported on the pyrolysed porous carbon matrix (Si@C) [49]. The resulting RH-derived Si@C hybrids exhibited desired properties for anode materials such as long-term cyclability and specific capacity of 600 mA × h/g at 2.0 A/g after 3700 cycles [49]. Afterward, Majeed et al. reported a similar process for the synthesis of Si/C nanocomposite from RH via calcination of RH to yield SiO_2/C which was then reduced to Si/C by metallic Al in molten salts at moderate temperatures [50]. The obtained Si/C composites showed a high reversible capacity of 1309 mA × h/g and a long-lasting durability (300 cycles) [50]. Likewise, Zhao et al. reported a low-temperature process for fabricating RH-Si/C via $AlCl_3$-assisted zincothermic reduction [51]. In this method, the biogenic SiO_2 in the SiO_2/C hybrid is converted into $SiCl_4$ which is subsequently reduced by metallic zinc powder to yield Si nanoparticles incorporated in the carbon matrix in the form of Si/C nano-hybrid [51]. Taking the intrinsic advantage of the inherent Si/C hybrid nature, Zhao et al. showed that the resulting RH-derived Si/C hybrid exhibited exceptional electrochemical behaviours with a capacity of 1033 mA × h/g achieved over 100 cycles under 1.0 A/g with 6.6 % capacity loss [51]. Under the condition of 2.0 A/g, the RH-derived Si/C hybrid preserved a capacity of 745 mA × h/g over 250 cycles, showing great potential for anode materials for Li-ion battery [51].

Tailoring RH-derived Si/C nanocomposites for better electrochemical behaviours is vital for the successful development of anode materials for Li-ion batteries. Zhang et al. fabricated hierarchically-shaped silicon/nitrogen-doped carbon nanotubes (CNTs) using a facile electrospray method (Fig. 5) [52]. The resulting hybrid material (Si/N@C) constituted silicon nanoparticles homogeneously supported on a highly conductive, porous N-doped carbon matrix, which enabled fast electronic transport and desirable durability during the lithiation/delithiation process [52]. Notably, the Si/N@C exhibited a high reversible specific capacity of 1380 mA × h/g at 0.5 A/g after 100 cycles, showing great potential for the next-generation rechargeable Li-ion battery [52]. Likewise, Yu et al. reported the synthesis of 3-D structured Si/C material from RH via magnesiothermic reduction [53]. Taking the

Table 1
RH-derived biogenic silica with tailored properties and potential applications.

Silica extraction methods	Featured properties of silica (purity, structure, etc.)	Potential applications	Sources
Alkaline-leaching in a boiling 0.1 M HCl solution	Ultrapure (apparently "absolute purity"), white, amorphous silica. No impurity detected by XRD pattern and EDX analysis.	Fillers for composite materials or concretes. Silicon fertilisers.	Nguyen et al. [10]
Acid-leaching using 2 M hydrochloric acid	RH-silica materials showed high silica content (> 85 % based on EDX or > 97 % based on XRF), good thermal stability. The obtained RH-silica showed great potential for applications in glass production, fillers for composite materials or adsorbents for metal ions removals.	Additives for glass productions. Fillers for composite materials. Adsorbents.	Aliyu et al. [41]
Comprehensive analysis of RH gasification	In-depth and comprehensive bibliometric analysis of the research landscape on rice husks gasification	Informative for decision-making processes.	Nyakuma et al. [42]
Leaching in a 0.032 M HCl solution at 70°C	Silica with 99.3 % purity as analysed using XRF. Iron oxide (α-Fe2O3) as impurity observed in XRD pattern	Catalyst supports for oxidation reactions.	Peralta et al. [43]
Alkaline-leaching using H_2SO_4, HCl, oxalic acid, and 1-butyl−3-methylimidazolium hydrogen sulfate.	H_2SO_4-leached was most efficient in terms of silica purity (99.6 wt%), followed by leaching using 1-butyl−3-methylimidazolium hydrogen sulfate (silica purity: 99.5 wt%). Leaching using 1-butyl−3-methylimidazolium hydrogen sulfate increased silica surface area and pore volume by a factor of 1.9 and 2.4, respectively, compared to the baseline.	Fillers for construction materials. Adsorbents.	Lee et al. [31]
RH-SiO_2 extraction via sonochemical method	Amorphous spherical RH-SiO_2 powder for potential applications as nano-biosensors and energy storage nano-devices. Tuning the sonication time enabled tailoring properties of the resultant silica such as particle size, porosity and bandgap. Increasing the sonication time from 0 to 50 min, the mean particle size augmented from 5 to 40 nm while the band gap dropped from 5.77 to 5.68 eV.	Potential for applications such as nano-biosensors and energy storage nano-device.	Sankar et al. [32]
Alkaline-leaching using NaOH solutions (5 and 10 wt%) in a reflux process followed by acid treatments with either 1 M HCl or 1 M acetic acid.	HCl showed superior effect compared to acetic acid with respect to the silica properties. HCl-based process produced silica with a surface area of 236 m^2/g and a porosity of 0.54 cc/g, much higher than the respective values of 204 m^2/g and 0.43 cc/g in the acetic acid-based process.	Potential for catalyst supports and adsorbents.	Dhaneswara et al. [33]
Alkaline extraction, acid-leaching and combustion.	RH-SiO_2 produced via alkali extraction was much more biocompatible than those produced via combustion or acid leaching processes.	Potential for biomedical applications.	Park et al. [34]
Different routes based on acid leaching, dissolution, and precipitation with the aid of surfactants.	Ordered mesoporous RH-silica with various topological shapes. Tuning silica structures by employing different synthesis routes based on acid leaching, dissolution, and precipitation with the aid of surfactants. Obtained RH-SiO_2 having various structural conformations (mesocellular forms, hexagonal nanochannels, irregular spherical, cylindrical aggregates), with a great diversity in the pore size, pore volume and specific surface area.	Potential for sustainable and environment-friendly industrial applications.	Chun et al. [35]
Controlling size and shape of RH-SiO_2 using polyethylene glycol and temperature adjustment during the precipitation step.	Achieved spherical silica particles with the sizes between ~250 nm and ~1.4 μm and the specific surface area over 200 m^2/g.	Potential applications in cosmetics, catalyst, biomaterial, and energy devices.	Kim et al. [36]
ZSM−5 zeolite using crystalline RHA as the precursor and organic template TPABr.	Obtained ZSM−5 with microporous structure and a high surface area of 397 m^2/g.	Potential for separation processes as sorbents. Catalyst for	Kordatos et al. [37]

(continued on next page)

Table 1 (*continued*)

Silica extraction methods	Featured properties of silica (purity, structure, etc.)	Potential applications	Sources
		petrochemical processes.	
Recover both the silica and carbon from RH.	1000 g of RH gave 119 g of fermentable sugar, 143 g of silica powder (grade >98 %, specific surface area of 328 m^2/g and 273.1 g of functional cellulose nano-fibrils (cellulose > 80.1 %).	Additives for paper, composites, packaging, coatings, biomedicine, and automobiles.	Jung et al. [38]
Alkaline peroxide leaching coupled with acid precipitation and ethanol extraction	Achieved bundles of micron-sized fiber-like cellulose and irregular-shape lignocelluloses products made of > 90 wt% carbon with 52.28 % crystalline fraction.	Potential for applications in green agriculture, environment, and biomaterials.	Nguyen et al. [39]
Selective dissolution, cyclic liquid nitrogen free-thaw, CO_2 supercritical drying	Dissolved RH in 1-butyl−3-methylimidazolium chloride, followed by a cyclic liquid nitrogen freeze-thaw process to produce a lignocellulose freeze gel which was then dried by a CO2 supercritical drying process to produce multi-functional self-assembled lignocellulose aerogel. Residue after the lignocellulose extraction was calcined to produce amorphous silica nanoparticles.	Potential for applications as catalyst supports, artificial muscles, supercapacitors, and absorbents.	Wei et al. [40]

advantage of the naturally conductive RH-derived carbon matrix for excellent electrochemical properties, the obtained 3-D structured Si/C material displayed remarkable cyclability 537 mA × h/g at 0.1 A/g after 200 cycles [53]. Chu et al. synthesized Si/C composite from RH using one-pot carbonization/magnesiothermic-reduction approach where they found that the higher carbonisation temperature led to better electrochemical properties of the resulting material [54]. Tao et al. reported a method for fabrication of RH-derived Si/C that minimises the need of costly metal reductants and stringent reaction environments [55]. Accordingly, the authors employed a reduction system based on CaH_2 and $AlCl_3$ for the in-situ low-temperature fabrication of a core-shell structured Si/C derived from RH [55]. The resulting core-shell Si/C hybrid showed exceptional cycling performance by maintaining 90.63 % capacity retention at 5 A/g over 2000 cycles [55]. Liu et al. fabricated Si@SiO_2/C anodes for Li-ion batteries using RH and waste coffee grounds (WCG) as feedstocks [56]. First, RH-SiO_2 is partially reduced via magnesiothermic method to produce Si@SiO_X nanocomposite which was then blended with WCGs and carbonised to yield Si@SiO_X/C as an anode material [56]. The obtained Si@SiO_X/C with the mass ratio (Si@SiO_X/C) = 1/2 showed a reversible capacity of 1125 mA × h/g at 0.1 A/g. Also, the Li-ion diffusivity increased from 2.7×10^{-12} cm^2/s in Si@SiO_X to 4.5×10^{-11} cm^2/s in Si@SiO_X/C, ascertaining the benefits of blending Si@SiO_X with WCG-derived carbon [56]. Notably, applying the Si@SiO_X/C (anode) and $LiNi_{0.5}Mn_{1.5}O_4$ (cathode) to a full cell yields to a high energy density of 396 W × h/kg, attesting the excellent performance of biowaster-derived Si@SiO_X/C as a low-cost and sustainable anode material [56]. Gautam et al. fabricated silicon/silicon carbide supported on carbon matrix (Si/SiC@C) from RH [57]. They showed that a certain fraction of the "SiC" phase in Si/SiC@C plays an intergral part in the creation of a stable interface, passivation of the Si surface, and suppression of Si cracking, which ultimately enhances battery cycling performance [57]. The best-obtained Si/SiC@C exhibited exceptional cycling stability up to 700 cycles with an areal capacity of ~2.3 mA × h/cm^2 at 0.2 A/g. The test cell consisting of the Si/SiC@C (anode) and NMC811 (cathode) displayed excellent capacity retention (>85 %) over 200 cycles [57].

Different RH-derived nanocomposites based on Si/C or SiO_2/C can be produced by tuning the synthesis conditions. Autthawong et al. found that these Si/C and SiO_2/C nanocomposites displayed different specific properties, for example, the SiO_2/C outperformed the Si/C in terms of cycling stability but was less effective than Si/C in terms of specific capacity [58]. Liao et al. reported a method for enhancing the coulombic efficiency of RH-Si/C materials by prelithiating with stabilised metallic Li powder [59]. They showed the Coulombic efficiency could be increased from 72.0 % in original RH-derived Si/C material to 95.1 % in prelithiated Si/C material. Moreover, the prelithiated Si/C electrode preserved its durability upon the Li intercalation/deintercalation cycles with a reversible capacity up to 1247.8 mA × h/g with 92.4 % capacity retention over 50 cycles [59]. Choi et al. indicated that RH-derived silicon nanowires could be produced via a molten salt process based on electrodeoxidation [60]. Adding NiO as an electric conductor enhanced the synthesis efficiency and generated pores in the silicon nanowires after washing [60]. The nanowires provided adequate free volume to accommodate the silicon electrode expansion and enabled the improvement in cycle life of the battery electrode [60]. Pereira et al. indicated that the formation of RH-SiC occurred when the carbonised RH was pyrolysed at the temperature of 1600 °C or higher [61]. At lower temperatures, the pyrolysis of carbonised RH led to the secondary formation of cristobalite, tridymite and quartz [61]. Featured achievements of developing RH-derived anode materials are tabulated in Table 2.

4. RH-derived materials for environmental remediation

RH-derived materials show great potential as effective and low-cost catalyst supports and/or adsorbents the environmental treatment and remediation. The biogenic RH-silica and/or RH-silica/carbon hybrid nanomaterials show substantial potential as catalyst support materials and adsorbents for environmental applications in green chemistry [62–68]. In particular, the inherent hybrid nature of RH-derived materials allows to produce catalysts or adsorbents with outstanding properties that are otherwise not achievable through synthetic means. In addition, the RH-derived support materials exhibit excellent compatibility with diverse catalysis-active components including transition metals, nobble metals, metal oxides, inorganic functional groups, organic functional groups and polymers. This excellent compatibility empowers the possibility to synthesize a wide range of catalysts with diverse catalytic functions.

4.1. Catalysts for decontamination of water and wastewater

Catalysts supported on RH-SiO_2 or RH-SiO_2/carbon hybrids present huge potential for the degradation of contaminants in water and wastewater. A wide variety of catalytically active components can be introduced to the surface of RH-SiO_2 or RH-SiO_2/carbon hybrids via chemical or physiochemical routes to produce various catalysts.

Metal catalysts supported on RH-SiO_2 (metal@RH-SiO_2) have gained the most interest. Typically, the conventional method for

Table 2
RH-derived anode materials for potential applications in lithium batteries.

RH-derived nanocomposites	Descriptions of materials as battery anodes	Sources
Si/C hybrid	Silicon nanocrystals possess low discharge potential and high specific capacity while the carbon matrix has high porosity and good electrical conductivity.	Sekar et al. [45]
Si/C hybrid	Flexible RH-derived carbon matrix creates a protective layer to compensate the volumetric variation of Si anode during lithiation/delithiation cycles.	Ma et al. [46]
Porous Si/C	RH-derived nanoporous silicon carbide with a high specific surface area (186.45 m^2/g) fabricated via magnesiothermic reduction at 950 °C. Silicon recovery efficiency: 88.46 %. Other products including potassium (yield: 91.5 %) and phosphorus (65.5 %).	Gao et al. [47]
Si/C composite	Si/C composite via carbonazation, ball milling, magnesiothermic reduction and additive treatment. Outstanding electrochemical behaviours: stable cycling with a high specific capacity retention of 572 mA × h/g at 1.0 A/g after 1000 cycles.	Li et al. [48]
Si@C hybrid nanocomposite	Si/C nanocomposite obtained via baking the precursor at 400 °C in air followed by reduction in molten $AlCl_3$. Crystalline Si nanoparticles supported on the porous carbon matrix (Si@C). Potential for anode materials: long-term cyclability and specific capacity of 600 mA × h/g at 2.0 A/g after 3700 cycles.	Lin et al. [49]
Si/C nanocomposite	Si/C nanocomposite: Calcinating RH for SiO_2/C and reducing SiO_2/C for Si/C by metallic Al in molten salts at moderate temperatures. High capacity (1309 mA × h/g) and long-lasting durability (300 cycles).	Majeed et al. [50]
Si/C hybrid composites	Low-temperature fabrication of Si/C via $AlCl_3$-assisted zincothermic reduction. Exceptional electrochemical behaviours: high capacity of 1033 mA × h/g over 100 cycles under 1.0 A/g with 6.6 % capacity loss. At 2.0 A/g, the Si/C maintained a capacity of 745 mA × h/g over 250 cycles.	Zhao et al. [51]
Si@N-doped/C	Hierarchically-shaped silicon/nitrogen-doped carbon/carbon nanotube sphere via electrospray method. Si nanoparticles homogenously supported on a highly conductive, porous N-doped carbon matrix. Fast electronic transport and good durability during lithiation/delithiation cycles. Reversible specific capacity of 1380 mA × h/g at 0.5 A/g after 100 cycles.	Zhang et al. [52]
3-D structured Si/C material	3-D structured Si/C material via magnesiothermic reduction. Remarkable cyclability 537 mA × h/g at 0.1 A/g after 200 cycles.	Yu et al. [53]
Si/C composite	Si/C composite using one-pot carbonization/magnesiothermic-reduction. Higher carbonisation temperature led to better electrochemical properties.	Chu et al. [54]
Core-shell structured Si/C hybrid	A core-shell structured Si/C hybrid via reduction of RH using CaH_2 and $AlCl_3$. Exceptional cycling performance by maintaining 90.63 % capacity retention at 5 A/g over 2000 cycles.	Tao et al. [55]
Si@SiO_2/C hybrid	RH-SiO_2 is partially reduced via magnesiothermic method to produce Si@SiO_X. Si@SiO_X was blended with waste coffee grounds (WCG) and carbonised to yield Si@SiO_X/C. Reversible capacity of 1125 mA × h/g at 0.1 A/g Li-ion diffusivity increased from 2.7×10^{-12} cm^2/s in Si@SiO_X to 4.5×10^{-11} cm^2/s in Si@SiO_X/C. Applying the Si@SiO_X/C (anode) and $LiNi_{0.5}Mn_{1.5}O_4$ (cathode) to a full cell yields a high energy density of 396 W × h/kg, attesting the excellent performance of biowaste-derived Si@SiO_X/C as a low-cost and sustainable anode material	Liu et al. [56]
Si/SiC@C hybrid	Silicon/silicon carbide supported on carbon matrix (Si/SiC@C). A certain fraction of the "SiC" phase in Si/SiC@C is crucial for the creation of a stable interface, passivation of the Si surface, and suppression of Si cracking, which ultimately enhances battery cycling performance Exceptional cycling stability up to 700 cycles with an areal capacity of ~2.3 mA × h/cm^2 at 0.2 A/g. Test cell consisting of Si/SiC@C (anode) and NMC811 (cathode) displayed excellent capacity retention (>85 %) over 200 cycles.	Gautam et al. [57]
Si/C and SiO_2/C nanocomposites	SiO_2/C outperformed Si/C in terms of cycling stability but was less effective than Si/C in terms of specific capacity.	Autthawong et al. [58]
Si/C composite	Enhancing the coulombic efficiency of Si/C materials by prelithiating with stabilised metallic Li powder. Coulombic efficiency increased from 72.0 % in original Si/C to 95.1 % in prelithiated Si/C. Prelithiated Si/C electrode preserved its durability upon the Li intercalation/deintercalation cycles with a reversible capacity up to 1247.8 mA × h/g with 92.4 % capacity retention over 50 cycles.	Liao et al. [59]
Silicon nanowires	RH-derived silicon nanowires produced via a molten salt process based on electrodeoxidation. Adding NiO as an electric conductor enhanced the synthesis efficiency and generated pores in the silicon nanowires after washing. The nanowires provided adequate free volume to accommodate the silicon electrode expansion and enabled the improvement in cycle life of the battery electrode.	Choi et al. [60]
Silicon carbide (SiC)	Formation of RH-SiC occurred when the carbonised RH was pyrolysed at the temperature of 1600 °C or higher. The pyrolysis of carbonised RH at lower temperatures led to the secondary formation of cristobalite, tridymite and quartz.	Pereira et al. [61]

metal@RH-SiO_2 synthesis consists of two main steps. Firstly, RH is treated by different means to produce the biogenic silica backbone with desired properties and structures as discussed in Section 3. In the next stage, the obtained silica is impregnated with catalytically active components such as metal precursors before being subjected to thermal treatments to create metal oxides as active sites on the silica substrates

[16]. Efforts were put on optimising experimental steps to simplify the catalyst synthesis procedure. Amongst those, the pioneering work can probably be accredited to Shen et al. who directly impregnated RH with metal salt solutions to produce metal-loaded biogenic silica for catalysis purposes [18]. Accordingly, RH was directly impregnated with $NiNO_3$ solution followed by the carbothermal reduction in an N_2 atmosphere to generate Ni@RH-SiO_2 catalyst [18]. The RHC nickel catalysts showed impressive catalytic performances, achieving up to 96.5 % tar conversion during copyrolysis with biomass. This is particularly important in biomass gasification, as tar formation is a major challenge due to its tendency to form complex hydrocarbons and hinder system performance. By converting tar in situ, the proposed method prevents macromolecular tar polymerization, which is a common issue in traditional biomass gasification [18]. Subsequently, Grimm et al. used a similar procedure to produce Mn@RH-SiO_2 catalyst [69]. This direct impregnation simplifies the catalyst synthesis procedure by incorporating the decarbonation and the metal incorporation in one single step. Hence, this direct impregnation method could be energy-efficient and cost-effective compared to the conventional two-stage approach discussed above.

A variety of metal@RH-SiO_2 catalysts with differences in catalytic activity has been produced by tuning the compositions and structures, which showed excellent performance in the decomposition of contaminants in wastewater and other applications in green chemistry. Fig. 6 provides an example of an Au@RH-SiO_2 catalyst [16]. The TEM image (a) shows the existence of Au clusters on RH-SiO_2 nanoparticles. The HRTEM image (b) provides a closer look at the sub-nanoscale structure of the Au clusters. This Au@RH-SiO_2 catalyst was found effective in catalysing the reduction of nitro compounds in water [16].

Catalytic reduction of contaminants in water based on metal@RH-SiO_2 has gained tremendous research interests. These reactions are relevant to various environmental and chemical synthesis processes. In addition, researchers also used these reactions as a case study to evaluate the catalytic activity of metal@RH-SiO_2 catalysts. Wang et al. reported the synthesis of Co-bearing catalysts in the form of nano metallic Co clusters on the RH-SiO_2 surface (Co@RH-SiO_2) [70]. They showed that the catalysts based on RH-derived SiO_2 displayed unique advantages compared to the ones based on commercial silica, for example, the RH-SiO_2-supported catalyst displayed more uniform pore sizes in between 2 and 4 nm, whereas the commercial SiO_2-supported catalyst showed irregular pore sizes [70]. Li et al. modified the surface of RH-SiO_2 with (3-aminopropyl)triethoxysilane to anchor the aminopropyl groups on RH-SiO_2 surface (i.e. amino@RH-SiO_2), which was then treated with Au precursor ($AuCl_4$) [16]. The adsorbed $AuCl_4$ was subjected to reduction process using $NaBH_4$ to produce metallic Au on the modified silica surface (Au/amino@RH-SiO_2), which exhibited an excellent catalytic activity in the reduction of 4-nitrophenol [16]. Similarly, Sinniah et al. reported the synthesis of Pt/amino@RH-SiO_2 using similar procedure, i.e. functionalising the RH-SiO_2 using aminoalkyl groups followed by introducing the Pt nanoparticles to the amino@RH-SiO_2 surface. The resulting Pt/amino@RH-SiO_2 catalyst showed potential for applications in the electrochemical reactions [67]. Fe/Ni@RH-SiO_2 was also found effective in catalysing the reduction of various nitro compounds with quite stable catalytic activity upon multiple reaction cycles, as per a study by Ghadermazi et al. [71]. Likewise, Ramya et al. synthesized CuO@RH-SiO_2 catalyst and tested it for the catalytic activity in reduction of 4-nitrophenol by $NaBH_4$ and antimicrobial ability against pathogenic microorganisms [72]. Lai et al. prepared Au/polyamide@RH-SiO_2 catalyst for the reduction of nitrophenol. The electroactive polyamide helped anchor Au nanoparticles to create an Au/polyamide hybrid material. The obtained catalyst enabled a conversion of > 95 % of nitrophenol to aminophenol [73]. Bogireddy et al. reported the synthesis of Pt/RH-SiO_2 and the effectiveness of this catalyst in catalysing degradation of 4-nitrophenol. In addition, the catalyst showed a good reusability with only 3 % loss of catalytic activity after eight cycles [74]. Vu et al. synthesized mesoporous Fe_2O_3@RH-SiO_2 composites for potential applications in the heterogeneous Fenton-like process [75]. They indicated that the resultant composite comprised 5 nm iron oxide particles (accounting for 8.1 wt% of composite mass) dispersed on the surface of RH-SiO_2 particles with a high specific surface area (109.5 m^2/g) [75]. This composite exhibited excellent capability of catalysing the degradation of tartrazine [75].

Wang et al. reported the synthesis of mesoporous TiO_2@RH-SiO_2 photocatalysts [76]. At the optimized calcination temperature of 700 °C, the obtained TiO_2@RH-SiO_2 photocatalyst displayed a mesoporous structure with a mean particle size of 22.75 nm and a specific surface area of 41.13 m^2/g [76]. The TiO_2 existed in the anatase phase and showed high catalytic activity for the removal of Rhodamine B in aqueous solutions under either the xenon lamp and sunlight irradiation. Moreover, TiO_2@RH-SiO_2 showed excellent ability for large-scale preparation, stable operation and recyclability [76].

RH-SiO_2/carbon hybrids supported catalysts: These catalysts are supported by RH-SiO_2/carbon hybrid materials derived from RH. As discussed above, apart from silica, RH also contains large fractions of cellulose and lignin which are also excellent catalyst support materials [62,77]. Unglaube et al. exploited the natural co-existence of carbon and silica in RH to derive nanostructured RH-SiO_2/carbon hybrid catalyst supports [62]. The intrinsic hybrid nature of RH-SiO_2/carbon nanocomposites results in functional catalysts which are otherwise difficult to make via synthetic means. Unglaube et al. successfully synthesized various catalysts based on RH-SiO_2/carbon hybrids using different metals such as silver, cobalt, nickel, and copper as the catalysis-active components [62]. When applied to the degradation reactions of aromatic and aliphatic nitro compounds, the Ag@RH-SiO_2/carbon by far outperformed the other studied catalysts based on cobalt, nickel, and copper. Fig. 7 illustrates a proposed mechanism for the degradation of nitro compounds on Ag@RH-SiO_2/carbon hybrids where clusters of Ag atoms as the catalytically active sites were deposited on the hybrid RH-SiO_2/carbon substrates [62]. Nitro compounds adsorbed on the catalyst surface, interacted with the active sites (Ag clusters) and decomposed through different stages as indicated in Fig. 7. Interestingly, Unglaube et al. found that Ag@SiO_2 catalysts (based on commercial silica) did not have any catalytic effects, ascertaining the crucial role of the hybrid nature of RH-SiO_2/carbon support materials in the catalytic activity of the catalysts [62]. In another study, Unglaube et al. found that Ni@RH-SiO_2 displayed excellent activity and selectivity for the conversion of olefin oxides to primary alcohols, showing great potential applications in the wastewater treatments and production of biofuels [64]. The benefits of RH-SiO_2/carbon nanocomposites as catalyst supports were consistently demonstrated by independent studies. For example, Madduluri et al. reported the superior performance of Ni@RH-SiO_2/carbon with Ni loading of 5 – 30 wt% for the

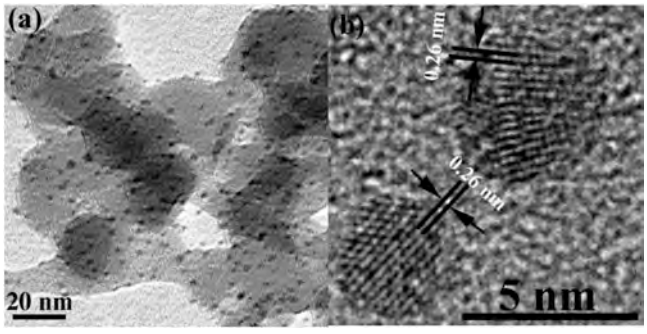

Fig. 6. Au catalysts supported on RH-SiO_2. TEM image (a) shows the existence of Au clusters on silica nanoparticles and HRTEM (b) reveals the structure of the Au clusters. Reproduced with permission from reference [16]. Copyright 2015 American Chemical Society.

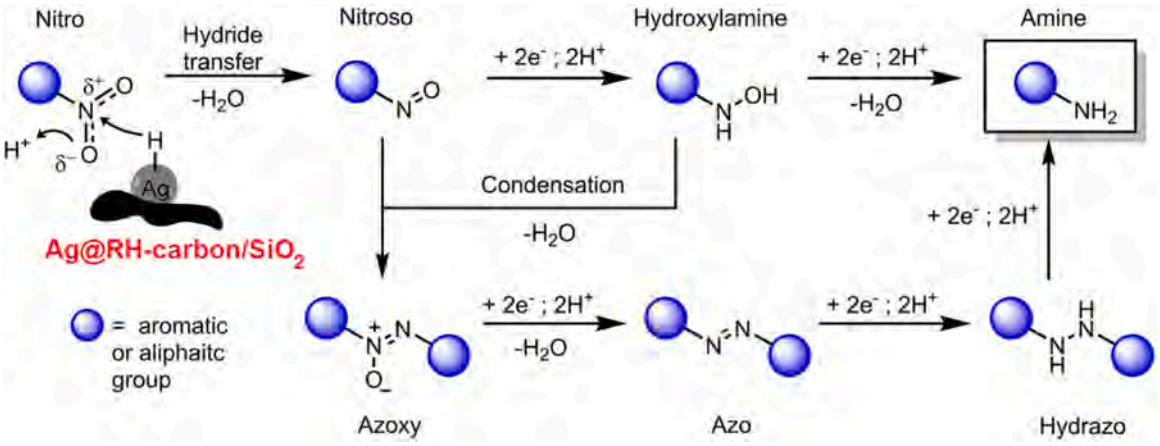

Fig. 7. Proposed mechanism of nitro compound reduction on a silver catalyst supported on a RH-carbon/SiO_2 hybrid (Ag@RH-carbon/SiO_2). Reproduced with permission from reference [62]. Copyright 2021 Wiley.

hydrogenation of biomass-derived molecules (e.g., levulunic acid and furfural) [78]. According to the authors, the Ni@RH-SiO_2/carbon with an optimal Ni loading of 15 wt% outperformed similar catalysts reported in the literature in the hydrogenation of both furfural and levulunic acid [78].

4.2. Catalysts for green transformation of gases

In addition to the above-discussed applications, metal@RH-SiO_2 catalysts also exhibited high catalytic activity in the reduction of gases related to green energy and environmental applications. For example, Balbuena et al. synthesized αFe_2O_3@RH-SiO_2 by calcination of $FeCl_3$-impregnated RH at 900 °C for a duration from 1 to 4 hours and achieved αFe_2O_3@RH-SiO_2 catalyst with only pure hematite (αFe_2O_3). The best obtained catalyst showed high catalytic activity in the photocatalytic oxidation of NO gas [79]. Likewise, Grimm et al. reported a high catalytic activity of Mn@RH-SiO_2 catalyst for the oxidation of CO gas [69].

Pastor et al. prepared ZnO@RH-SiO_2 by calcination of the zinc acetate-impregnated RH at 600 °C, yielding ZnO nanoparticles (70–180 nm) on RH-SiO_2 surface [80]. The resulting ZnO@RH-SiO_2 catalyst had a specific surface area up to 53 m^2/g and a band gap of ~3.1 eV. The authors used this material as a cost-effective and sustainable photocatalyst for decomposition of NO_X gases [80]. Under the sunlight irradiation, the ZnO@RH-SiO_2 was found to catalyse the decomposition of NO gas through the following pathway $NO \rightarrow HNO_2 \rightarrow NO_2 \rightarrow NO_3^-$ with a high NOX removal rate (70 %) and excellent selectivity (>90 %). The authors indicated that the ZnO@RH-SiO_2 outperformed the unsupported ZnO and the standard TiO_2/P25 catalysts due to the beneficial effect of RHA as a template, which allowed smaller and well dispersed ZnO particles. Also, ZnO@RH-SiO_2 showed good recyclability and reusability after four consecutive runs [80].

4.3. Catalysts for green chemistry synthesis

Non-metal catalysts: Apart from metal-based catalysts, the RH-SiO_2 showed an excellent compatibility with various non-metal catalytic functional groups. The resulting non-metal@RH-SiO_2 displayed a high catalytic activity in a wide range of reactions. For example, Janaun et al. reported the synthesis of sulfonic acid-functionalized RH-SiO_2 ($-SO_3H$@RH-SiO_2) and showed that this catalyst performed effectively in the esterification reaction between oleic acid and methanol [68]. Likewise, Lolage et al. showed that the $-SO_3H$@SiO_2 catalysts used in the acetylation of benzyl alcohol, exhibited over 99 % selectivity towards benzyl acetate as a desired product [81].

Moreover, a huge volume of research has focused on the synthesis and test of organic-functionalised RH-SiO_2 for catalysts. For example, Zare et al. modified the RH-SiO_2 by grafting 4,4′-bipyridine scaffold on its surface and applied the obtained catalytic nanomaterial for the synthesis of pyrano[2,3-*d*]pyrimidine-2,4-diones and pyrano(2,3-d) pyrimidine-4-one-2-thiones from aromatic aldehyde, malononitrile and barbituric acid [82]. They reported a high catalytic activity of the surface-modified RH-SiO_2 for these reactions. Elimbinzi et al. synthesized mesoporous micelle templated rice husk silica (MT-RHS) using sodium silicate derived from rice husk ash, with castor oil serving as a renewable surfactant template.[83]. Functionalizing the synthesized MT-RHS with organo-amines (primary amine APTS and tertiary amine DEPA) produced effective solid base catalysts. These catalysts demonstrated high activity for the low-temperature transesterification of C4–C12 triglycerides (TAGs) into fatty acid methyl esters (FAMEs), a key step in biodiesel production. Notably, the DEPA-MT-RHS catalyst showed significantly higher activity than the primary amine-functionalized materials, providing a five-fold rate enhancement for certain reactions.[83]. The DEPA-MT-RHS catalyst exhibited moderate recyclability, with only a 10 % decrease in activity after the first reuse and a 50 % decrease after five cycles. The versatility of the catalyst was also demonstrated by its ability to effectively transesterify longer-chain triglycerides (C8 and C12), with high FAME selectivity. [83]. Hakkim et al. prepared nitrone-functionalised RH-SiO_2 for polymer grafting through spin capturing and 1,3-dipolar cycloaddition mechanisms, and demonstrated the advantages of using nitrone@RH-SiO_2 catalysts for the polymer grafting practices [84]. In a comparative study, Pandey et al. studied two different functional moieties, namely a base (3-aminopropyl)triethoxysilane (APTES) and an acid (3-mercaptopropyl)triethoxysilane (MPTES), for functionalising RH-SiO_2 supports [85]. They found that the base APTES@RH-SiO_2 outperformed the acid MPTES@RH-SiO_2 in the ring-opening reactions of various oxiranes [85]. Specifically, when the base APTES@RH-SiO_2 was applied to ring-opening reactions of morpholine and piperidine, the corresponding conversion reached 93 and 91 %, respectively, whereas the respective values for the acid MPTES@RH-SiO_2 were only 52 and 57 % [85]. Jamnongphol et al. fabricated RH-SiO_2 as a support for zirconocene/MMAO catalyst in ethylene polymerisation (zirconocene/MMAO@ RH-SiO_2) [86]. The obtained biogenic RH-SiO_2 displayed a larger surface area and higher purity than commercial silica. Moreover, the RH-SiO_2 showed compatibility with the catalysis-active MMAO component, leading to a good distribution of MMAO over the support surface [86]. As such, the zirconocene/MMAO@RH-SiO_2 exhibited a higher catalytic activity the polymerization reactions than the commercial catalysts [86]. Jin et al. fabricated Fe/N@RH-carbon electrocatalyst via doping Fe-containing salt coupled with high-temperature NH_3 etching and doping [87]. They obtained Fe/N@RH-carbon showed

an amorphous carbon structure uniformly embedded by nanometal particles, and displayed high catalytic activity in oxygen reductions [87]. When applied to zinc-air battery, the Fe/N@RH-carbon composite displayed a 1.4 V open-circuit voltage and high peak power density (156.1 mW/cm^2), attesting potential for a low-cost and renewable electrocatalytic material for energy conversion and storage [87].

Biocatalysts: Owing to its biogenic nature, RH-SiO_2 presents an ideal support material for biocatalysts. A large body of research has devoted to realising this unique potential of RH-SiO_2. For example, Gama et al. prepared phenyl-grafted RH-SiO_2 for the immobilisation of lipase [88]. Lipase is an essential enzyme that catalyses the degradation of triglycerides (a common type of fats) into free fatty acids and glycerol, and thus, plays a central role in various biological, natural, industrial and environmental systems [89–92]. Gama et al. indicated that the resulting lipase/phenyl@RH-SiO_2 biocatalyst with an enzyme loading of ~27.7 mg/g displayed high catalytic activity in the hydrolysis of olive oil emulsion or the synthesis of cetyl oleate related to cosmetic industry [88]. Machado et al. immobilised lipase on RH-SiO_2 functionalised by triethoxy(octyl)silane [93]. The resulting lipase/octyl@RH-SiO_2 biocatalyst with an enzyme loading of 22 mg/g showed remarkable catalytic activity in the production of wax esters via esterification reactions in a heptane medium. Also, the lipase/octyl@RH-SiO_2 biocatalyst experienced a slight loss of 10 – 15 % in activity after nine successive cycles [93]. In a comparative study, Sabi et al. showed that functionalising the RH-SiO_2 with appropriate alkyl groups prior to enzyme loading led to a significant improvement of the durability of biocatalysts compared to the ones without the alkyl functionalising step [94]. Mori at al synthesized rose bengal-impregnated rice husk nanoparticles [95]. Rose bengal belongs to halogenated xanthenes that act as photosensitiser with superior photophysical properties. Modifying RH-SiO_2 surface with cationic polyethyleneimine was found to enhance the adsorption of the anionic rose Bengal [95]. The resulting rose-bengal/amine@RH-SiO_2 enabled the antimicrobial photodynamic inactivation of bacteria related to dental applications [95]. Featured achievements of developing RH-derived catalysts for environmental remediation and green chemistry are tabulated in Table 3.

4.4. Decontamination via RH-adsorbents

Apart from catalysts, RH-derived adsorbents (RH-adsorbents) open an efficient and low-cost pathway for water and wastewater treatments [19,20] as well as separation and purification of gas mixtures [113]. Similar to the case of catalyst applications, the hybrid nature of RH-SiO_2/carbon hybrids presents an exceptional advantage as multifunctional adsorbents which showed effectiveness in adsorbing both inorganic and organic contaminants, including heavy metal cations, inorganic ions and organic compounds. This unique potential of RH-adsorbents has entailed enduring research interests in this field.

Removal of organic matter. RH-adsorbents displayed effective removal of various forms of organic matter in aqueous environments. For example, Villota-Enríquez et al. reported the synthesis of RH-adsorbents with amorphous and aggregated submicron particles (<200 nm) and specific surface area of ~202.31 m^2/g, which showed a high capability of removal of methylene blue from wastewater [96]. They also indicated that combining the chemical treatment with 2 N HCl solution and UV irradiation resulted in RH-adsorbents with a remarkable enhancement in the methylene blue adsorption capacity [96]. Islam et al. reported the successful preparation of two RH-adsorbents by chemically modifying RHA for decontaminating crystal violet dye in wastewater [97]. The resulting RH-adsorbents, called carbon embedded silica and RHA-mediated zeolite, showed the specific surface area values of 110 and 122 m^2/g, respectively, which are significantly higher than that of unmodified RHA (28 m^2/g) [97]. Consequently, the two RH-adsorbents showed a much higher crystal violet dye adsorption capacity of 18.75 mg/g and 19.28 mg/g respectively, compared to that of

Table 3
RH-derived materials for applications as catalysts and adsorbents for environmental remediation and green chemistry.

Catalysts/adsorbents(*)	Reactions and notes	Source
Co@RH-SiO_2 (Catalyst)	Co@RH-SiO_2 catalyst displayed more uniform pore sizes in 2–4 nm, whereas the commercial SiO_2-supported catalyst showed irregular pore sizes.	Wang et al. [70]
Au/amino@RH-SiO_2 (Catalyst)	Reduction of 4-nitrophenol. The Au/amino@RH-SiO_2) exhibited an excellent catalytic activity in the reduction of 4-nitrophenol.	Li et al. [16]
Pt/amino@RH-SiO_2 (Catalyst)	Electrochemical reaction in fuel cells: Functionalising RH-SiO_2 using aminoalkyl groups followed by introducing Pt nanoparticles to the resulting amino@RH-SiO_2 surface. The Pt/amino@RH-SiO_2 showed potential for electrochemical reactions.	Sinniah et al. [67]
Fe/Ni@RH-SiO_2 (Catalyst)	Reduction of various nitro compounds with quite stable catalytic activity upon multiple reaction cycles.	Ghadermazi et al. [71]
CuO@RH-SiO_2 (Catalyst)	Reduction of 4-nitrophenol and antimicrobial activity against pathogenic microorganisms.	Ramya et al. [72]
Ni@RH-SiO_2 (Catalyst)	Gasification of biomass with a biomass conversion reached 96.5 %. Catalyst synthesized via simplified one-step direct impregnation method.	Shen et al. [18]
αFe_2O_3@RH-SiO_2 (Catalyst)	Photocatalytic oxidation of NO with the highest NO conversion of 24 %.	Balbuena et al. [79]
TiO_2@RH-SiO_2 (Catalyst)	High catalytic activity for removal of Rhodamine B in aqueous solutions under either the xenon lamp and sunlight irradiation.	Wang et al. [76]
Mn@RH-SiO_2 (Catalyst)	CO oxidation reaction. The Mn@RH-SiO_2 catalyst exhibited high catalytic activity in the reduction of CO gas.	Grimm et al. [69]
ZnO@RH-SiO_2 (Catalyst)	Decomposition of NO gas: NO → HNO_2 → NO_2 → NO_3^- with a high NO_X removal rate (70 %) and excellent selectivity (>90 %). ZnO@RH-SiO_2 outperformed the standard TiO_2/P25 catalysts.	Pastor et al. [80]
Au/polyamide@RH-SiO_2 (Catalyst)	Reduction of nitrophenol with a conversion of > 95 % of nitrophenol to aminophenol.	Lai et al. [73]
Pt/RH-SiO_2 (Catalyst)	Degradation of 4-nitrophenol. Good catalytic activity and good reusability with only 3 % loss of catalytic activity after eight cycles.	Bogireddy et al. [74]
Metal@RH-carbon/SiO_2 (Metal = Ag, Cu, Co, Ni) (Catalyst)	Hydrogenation of both aromatic and aliphatic nitro compounds. Ag@RH-carbon/SiO_2 by far outperformed the other catalysts. Similar catalysts based on commercial SiO_2 didn't work, ascertaining a crucial role of the hybrid nature of RH-derived supports.	Unglaube et al. [62]
Ni@RH-SiO_2 (Catalyst)	Ring-opening hydrogenation of epoxides. Ni@RH-SiO_2 performed multimodes of catalytic activity	Unglaube et al. [64]

(continued on next page)

Table 3 (*continued*)

Catalysts/adsorbents(*)	Reactions and notes	Source
	as Brønsted acid, Lewis acid and hydrogenation catalyst. The Ni@RH-SiO_2 catalysed the selective anti-Markovnikov ring-opening hydrogenation of epoxides to primary alcohols.	
$-SO_3H$@RH-SiO_2 (Catalyst)	Esterification: between oleic acid and methanol.	Janaun et al. [68]
	Acetylation of benzyl alcohol, showing over 99 % selectivity towards benzyl acetate.	Lolage et al. [81]
Amino@RH-SiO_2 vs. Mercapto@RH-SiO_2 (Catalyst)	Ring-opening of oxiranes: The base amino@SiO_2 catalyst outperformed the acid mercapto@SiO_2 catalyst.	Pandey et al. [85]
Zirconocene/MMAO@ RH-SiO_2 (Catalyst)	Ethylene polymerisation: Excellent compatibility between RH-SiO_2 and MMAO ensures uniform distribution of MMAO over the support surface. Zirconocene/MMAO@RH-SiO_2 showed a higher catalytic activity than commercial catalysts	Jamnongphol et al. [86]
Fe/N@RH-carbon (Catalyst)	Oxygen reductions: Fe/N@RH-carbon electrocatalyst via doping Fe coupled with high-temperature NH_3 etching and doping. Amorphous carbon structure uniformly embedded by nanometal particles with high catalytic activity in oxygen reductions. When applied to zinc-air battery, Fe/N@RH-carbon displayed a 1.4 V open-circuit voltage and high peak power density (156.1 mW/cm^2), attesting potential for a low-cost and renewable electrocatalytic material.	Jin et al. [87]
Bipyridine@RH-SiO_2 (Catalyst)	Synthesis of pyrano(2,3-d) pyrimidine−2,4-diones and its variants from aromatic aldehyde, malononitrile and barbituric acid	Zare et al. [82]
Nitrone@RH-SiO_2 (Catalyst)	Polymer grafting via spin capturing and 1,3-dipolar cycloaddition reactions	Hakkim et al. [84]
Amine@mesoporous templated RH-SiO_2 (Catalyst)	Transesterification reactions of triglycerides to methyl laurate relevant to biodiesel synthesis. The templated silica showed a better function than the ordinary one.	Elimbinzi et al. [83]
Lipase immobilised on phenyl@RH-SiO_2	Immobilisation of lipase and hydrolysis of olive oil emulsion; synthesis of cetyl oleate.	Gama et al. [88]
Lipase immobilised on octyl@RH-SiO_2 (Catalyst)	Esterification for the production of wax esters in a heptane environment. 10–15 % loss of catalytic activity after nine cycles.	Machado et al. [93]
Lipase/alkyl@RH-SiO_2 vs. Lipase@RH-SiO_2 (Catalyst)	Functionalising the RH-SiO_2 with appropriate alkyl groups prior to enzyme loading improves the durability of biocatalysts, compared to the ones without the alkyl functionalising step.	Sabi et al. [94]
RH-SiO_2 (Adsorbent)	Removal of methylene blue from wastewater. Combining chemical treatment with 2 N HCl solution and UV irradiation yielded RH-adsorbents with enhanced adsorption capacity.	Villota-Enríquez et al. [96]
Carbon-embedded RHA versus RHA-mediated zeolite (Adsorbent)	Decontaminating crystal violet dye in wastewater. Carbon-embedded RHA and RHA-mediated zeolite had a surface area of 110 and 122 m^2/g, respectively, surpassing RHA (28 m^2/g). Carbon-embedded RHA and RHA-mediated zeolite showed a crystal violet dye adsorption capacity of 18.75 mg/g and 19.28 mg/g respectively, outperforming RHA (8.3 mg/g).	Islam et al. [97]
TiO_2@RHA (Adsorbent/catalyst dual function)	Removal of bisphenol-A from aqueous environments. TiO_2@RHA alone removed 34.5 % of bisphenol-A. TiO_2@RHA coupled with UV light irradiation removed 97.6 % of bisphenol-A within 1 hour.	Thuan et al. [98]
RHA versus Fe@RHA (Adsorbent)	Removal of dimethylated arsenicals. RHA and Fe@RHA adsorbed inorganic arsenate at 1.28 and 6.32 mg/g, respectively. RHA didn't adsorb organic arsenics but Fe@RHA adsorbed dimethylarsinic acid (at 7.08 mg/g), dimethylmonothioarsinic acid (0.43 mg/g)and dimethyldithioarsinic acid (0.28 mg/g).	Yoon et al. [99]
RHA, RH-SiO_2 and UV-assisted RH-SiO_2 (Adsorbent)	Methylene blue (MB) removal: RHA without chemical pre-treatment of the initial RH precursor removed only 30 % of MB from the aqueous solution. Pre-treating the RH precursor with a 3 N HCl solution before calcination led to RH-SiO_2 with an amorphous structure and a specific surface area of 202 m^2/g, which increased the MB removal efficiency to 50 %. Pre-irradiating RH-SiO_2 with UV for 5 min boosted the MB removal efficiency to 73 %.	Villota-Enríquez et al. [100]
RH-mesoporous silicon (Adsorbent)	Methylene blue (MB) removal: An excellent maximum MB sorption capacity of 213.31 mg/g based on Sips model. RH-mesoporous silicon showed a strong preference toward adsorbing MB from a binary system containing both MB and Rhodamine B.	Hou et al. [101]
RH-chitosan-SiO_2/$CaCO_3$ (Adsorbent)	Escherichia coli (E. coli) removal: RH-chitosan-SiO_2/$CaCO_3$ synthesized using RH (for chitosan-silica) and waste eggshells (for $CaCO_3$). The hybrid removed 80 % of Escherichia coli after 35 min of incubation.	Bwatanglang et al. [102]
RH-SiO_2 (Adsorbent)	Fluoride removal from water and wastewater: RH-SiO_2 showed a exceptional efficiency in fluoride removal with adsorption capacity of 12 mg/g.	Pillai et al. [103]

(*continued on next page*)

Table 3 (*continued*)

Catalysts/adsorbents(*)	Reactions and notes	Source
Burning-derived RHA and calcination-derived RHA (Adsorbent)	Rhodamine B (RB) removal: Burning-derived RHA showed a better capability of removing RB from aqueous solutions (at removal efficiency of 84 % after 24 hours) compared to that of the calcination-derived RHA (at 60 %).	Tsamo et al. [104]
SBA−16 mesoporous RH-SiO_2 (Adsorbent)	Rhodamine B (RB) removal: SBA−16 RH-SiO_2 with an amorphous ordered mesoporous structure and a surface area of 461 m^2/g showed a maximum RB adsorption capacity of 166.7 mg/g as based on Langmuir model.	El-Shafey et al. [105]
RHA/alumina composite	Uranium removal from aqueous solutions: RHA/alumina composite showed a uranium removal efficiency of 96.35 %.	Youssef et al. [106]
RH-SiO_2/chitosan nanocomposite (Adsorbent)	Removal of $^{152+154}$Eu+154 radionuclide from aqueous environments: Coating RH-SiO_2 surface with chitosan to yield RH-SiO_2/chitosan nanocomposite. The composite adsorbed $^{152+154}$Eu+154 radionuclide from aqueous environments at a capacity of 160 mg/g at pH = 5 and 298 K.	Dakroury et al. [107]
γFe_2O_3@RH-SiO_2 (Adsorbent)	Removal of Ni(II) ions in water: γFe_2O_3@RH-SiO_2 was fabricated using ferrate as an internal oxidation modifier. This adsorbent removed 96.1 % of Ni(II) ions within 24 h, yielding a maximum adsorption capacity is 42.69 mg/g at room temperatures and neutral pH.	Nie et al. [108]
Alginate@RHA (Adsorbent)	Removal of Pb(II) ions in wastewater: Alginate@RHA showed a BET surface area (120 m^2/g) and the total pore volume (0.653 cm^3/g). Alginate@RHA showed a Pb(II) adsorption capacity of 112.3 mg/g and kinetics of Pb (II) removal of 0.0081 mg/g per min, far surpassing unmodified RHA at 41.2 mg/g and 0.00025 mg/g per min, respectively. Alginate@RHA removed over 99 % of Pb(II) from wastewater with a good recyclability.	Pham et al. [109]
Chlorinated RHA (Adsorbent)	Mercury removal: The surface area and pore volume of the chlorinated RHA increased with increasing chlorination temperature. Under chlorination at 1000 °C for 10 min, the chlorinated RHA had a surface area of 335 m^2/g and a maximum mercury adsorption capacity of 620 mg/g.	Mochizuki et al. [110]
Phenylamine@RH-SiO_2 (Adsorbent)	Removal of Ni(II) ions in aqueous solutions: Hybrid adsorbent based on ortho-phenylenediamine embedded on RH-SiO_2. The amine@RH-SiO_2 showed good uptake of Ni(II) from aqueous solutions.	Abbas et al. [111]
Polyethyleneimine@RH-SiO_2 (Adsorbent)	Phosphate removal from wastewater: Grafting branched polyethyleneimine onto RH-SiO_2 yielded to polyethyleneimine@RH-SiO_2 which absorbed phosphate at 123.46 mg/g, a two-fold greater than that of untreated RH-SiO_2.	Suzaimi et al. [112]

unmodified RHA (8.3 mg/g) [97]. Thuan et al. reported the synthesis of TiO_2@RHA for the removal of bisphenol-A micropollutant in wastewater [98]. They showed that the TiO_2@RHA could remove 34.5 % of bisphenol-A from the aqueous environments in dark media but the removal efficiency increased remarkably to 97.6 % within 1 hour under UV light-irrediated conditions, which provided a 2-fold increase in the removal efficiency compared to that of standard commercial TiO_2, attesting the benefits of RH-derived supports [98]. Yoon et al. studied the adsorption of dimethylated arsenicals on RHA and Fe@RHA using isothermal adsorption procedures combined with X-ray absorption spectroscopy [99]. They derived the adsorption capacity of 1.28 and 6.32 mg/g for inorganic arsenate adsorption on RHA and Fe@RHA, respectively. No adsorption of dimethylated arsenicals was found on RHA while Fe@RHA showed a good capability of adsorbing organic arsenics with the adsorption capacity of 7.08 mg/g for dimethylarsinic acid, 0.43 mg/g for dimethylmonothioarsinic acid and 0.28 mg/g for dimethyldithioarsinic acid [99]. The beneficial role of Fe@RHA was attributed to the formation of iron oxide in the form of two-line ferrihydrite on RHA surface which acted as the adsorption sites [99]. Villota-Enríquez et al. showed that RHA without chemical pre-treatment of the initial RH precursor showed a limited capacity of methylene blue adsorption (i.e., could only remove 30 % of methylene blue from the aqueous solution) [100]. Pre-treating the RH precursor with 3 N HCl solution before the calcination process led to RH-SiO_2 with an amorphous structure in the form of highly agglomerated submicron particles (<200 nm) and a specific surface area of 202 m^2/g, which could increase the methylene blue removal efficiency to 50 % [100]. Furthermore, pre-irradiating the RH-SiO_2 with UV for 5 min could boost the methylene blue removal efficiency to 73 % [100]. Hou et al. reported the synthesis of RH-mesoporous silicon that showed an excellent maximum methylene blue sorption capacity of 213.31 mg/g based on Sips model [101]. In addition, the RH-mesoporous silicon showed a strong preference toward adsorbing methylene blue from a binary system containing both methylene blue and Rhodamine B [101]. Bwatanglang et al. synthesized a hybrid adsorbent based on chitosan-silica/calcium carbonate using RH (for chitosan-silica) and waste eggshells (for calcium carbonate) [102]. The resulting RH-chitosan-SiO_2/$CaCO_3$ could remove 80 % of Escherichia coli (E. coli) after 35 min of incubation [102]. Pillai et al. derived RH-SiO_2 as inexpensive and efficient adsorbent for fluoride removal from water and wastewater [103]. The resulting RH-SiO_2 showed good efficiency in fluoride removal with adsorption capacity of 12 mg/g [103]. Tsamo et al. compared the adsorption performances of two RHA obtained by different decarbonation routes, i.e. combustion-derived RHA via burning raw RH in open air and calcination-derived RHA via calcining raw RH in a Muffle Furnace at 540 °C [104]. The burning-derived RHA showed a better capability of removing Rhodamine B from aqueous solutions (with a removal efficiency of 84 % after 24 hours) compared to that of the calcination-derived RHA (at 60 %) under similar adsorption conditions [104]. Likewise, El-Shafey et al. prepared SBA-16 mesoporous RH-SiO_2 for Rhodamine B uptake from aqueous media [105]. They obtained SBA-16 RH-SiO_2 displayed an amorphous ordered mesoporous structure and a total surface area of 461 m^2/g, and a maximum Rhodamine B adsorption capacity of 166.7 mg/g as based on Langmuir model [105].

Removal of heavy metal ions. Owing to their hybrid nature, RH-SiO_2/carbon nanocomposites are multifunctional adsorbents, which are effective for not only organic matter removal but also heavy metal ion adsorption. Youssef et al. synthesized a RHA-alumina composite for removal of uranium from aqueous solutions and reported a uranium adsorption efficiency of 96.35 % for this composite adsorbent [106]. Dakroury et al. synthesized RH-nanosilica via the thermal treatment coupled with acid leaching route followed by the coating of silica surface with chitosan gel to yield a RH-SiO_2/chitosan nanocomposite [107]. The material was found capable of adsorbing $^{152+154}$Eu+154 radionuclide from aqueous environments at a capacity of 160 mg/g at pH = 5 and 298 K [107]. Nie et al. prepared γFe_2O_3@RH-SiO_2 using ferrate as an internal oxidation modifier [108]. They showed that the resulting γFe_2O_3@RH-SiO_2 exhibited an excellent capacity for the adsorption of Ni(II) ions in water. At room temperatures and neutral pH, this adsorbent could remove 96.1 % of Ni(II) ions within 24 h, corresponding to a maximum adsorption capacity is 42.69 mg/g [108]. Pham et al. synthesized alginate@RHA for removal of Pb(II) ions in wastewater [109]. The resulting alginate@RHA showed a remarkable enhancement in the high BET specific surface area (120 m^2/g) and the total pore volume (0.653 m^3/g) compared to the ordinary RHA [109]. This morphological improvement entailed an increase in the adsorption capacity (112.3 mg/g) and kinetics of Pb(II) removal (0.0081 mg/g per minute), compared to the corresponding values obtained of unmodified RHA at 41.2 mg/g and 0.00025 mg/g per minute, respectively. The alginate@RHA could remove over 99 % of Pb(II) from wastewater with a good recyclability [109]. Mochizuki et al. reported the synthesis of silicone tetrachloride ($SiCl_4$) from RHA by chlorination for applications as mercury removal [110]. The surface area and pore volume of the chlorinated RHA showed increasing trends with increasing chlorination temperature [110]. At chlorination of 1000 °C for 10 minutes, the resulting chlorinated RHA exhibited a surface area of 335 m^2/g and a maximum mercury adsorption capacity of 620 mg/g [110].

In parallel to tuning the synthesis process for desired compositions and structures, efforts have been put on surface engineering to improve the functionality of RH-adsorbents. For example, Abbas et al. reported the successful synthesis of a hybrid adsorbent based on RH-SiO_2 and ortho-phenylenediamine, which showed a good uptake of Ni(II) ions in aqueous solutions [111]. Likewise, Suzaimi et al. indicated that grafting branched polyethyleneimine onto RH-SiO_2 resulted in an improvement in the selective uptake of phosphate in wastewater [112]. Under similar experimental conditions, the polymer-grafted RH-SiO_2 showed a phosphate adsorption capacity of 123.46 mg/g which was twice times higher than that of the RH-SiO_2 without surface treatments [112]. Featured achievements of developing RH-derived adsorbents for environmental remediation are tabulated in Table 3.

5. RH-derived materials for hydrogen production

Hydrogen plays an integral part in the roadmap of energy transition towards the low-carbon future [114–117]. To date, most hydrogen is produced via catatytic processes such as gas reforming, gasification of solid mass (coals, biomass), water-gas shift reaction, and decomposition of hydrocarbons. Conventional methods for hydrogen production generate CO_2 as a co-product in addition to hydrogen. Hence, additional carbon capture and storage (CCS) is required to achieve the net-zero emissions target [118,119]. Notably, catalytic decomposition of hydrocarbons is the only technology that can avoid CO_2 emissions and, thus, enable the negative emission economy. In particular, methane-derived hydrogen presents a long-lasting clean energy owing to the plentiful sources of methane in the forms of natural gas in underground reservoirs as well as abundant methane-bearing gas hydrates in the seafloors and permafrost sediments [120–123]. The potential of RH-derived catalysts for applications in these crucial areas will be discussed in this section.

Catalytic decomposition of hydrocarbons. As mentioned above, this catalytic decomposition of hydrocarbons presents a very desirable technology for hydrogen production as it entails no CO_2-emission. However, a standing challenge for this method is the ongoing deactivation of the catalysts due to the continuing deposition of solid carbon resulting from the decomposition reactions [124]. Fig. 8 shows selected images recorded by Yun et al. to exemplify the deactivation of the catalysts in methane decomposition due to carbon deposition. The surface of the pristine catalysts was smooth (Fig. 8a), yet the used catalysts had a very rough surface due to solid carbon deposition (Fig. 8b) [124]. The TEM images provide a magnified view to confirm the even surface of pristine catalyst (8c) and the emergence of a wrinkled-graphene layer on the used catalyst (Fig. 8d) [124]. Interestingly, several studies indicated that RH-derived catalysts based on the inherent carbon/RH-SiO_2 hybrids displayed a remarkable tolerance to the carbon deposition issue and thus exhibited a better durability compared to other catalysts [17]. This is another piece of solid evidence attesting the extraordinary beneficial feature of RH-derived materials.

Active studies have focused on developing RH-catalysts for catalytic decomposition of hydrocarbons (e.g., methane and biomass). Gómez-Pozuelo et al. reported the synthesis of different RH-SiO_2 materials sourced exclusively from RH (without incorporating any non-RH materials) and used these materials as catalysts for the decomposition of methane for hydrogen generation (Fig. 9) [17]. They indicated that RH-SiO_2 with larger BET surface area and amorphous structure displayed the highest catalytic activity. Interestingly, Gómez-Pozuelo et al. indicated that RH-SiO_2 obtained from acid-leaching process showed a remarkable resistance against deactivation, without no considerable loss in catalytic activity in a long-time operation [17]. Zhao et al. synthesized RH-SiO_2 and Ni@RH-SiO_2 using a sol–gel process and tested the resulting materials for catalytic performance on the methane decomposition reactions. The RH-SiO_2 without loading nickel moderate catalytic activity in the methane decomposition with a methane conversion efficiency up to 38.83 %. After being incorporated with nickel particles as catalysis-active sites, the resulting Ni@RH-SiO_2 catalyst showed an effective performance with a methane conversion efficiency up to 74.33 % [125]. In a comparative study, Farooq et al. compared different methods for the preparation of Ni@RH-SiO_2 for catalysing the steam gasification reactions [126]. They showed that the best obtained Ni@RH-SiO_2 enabled a maximum hydrogen generation of 0.471 mol/(g feedstock × g catalyst). The Ni@RH-SiO_2 exhibited a much better

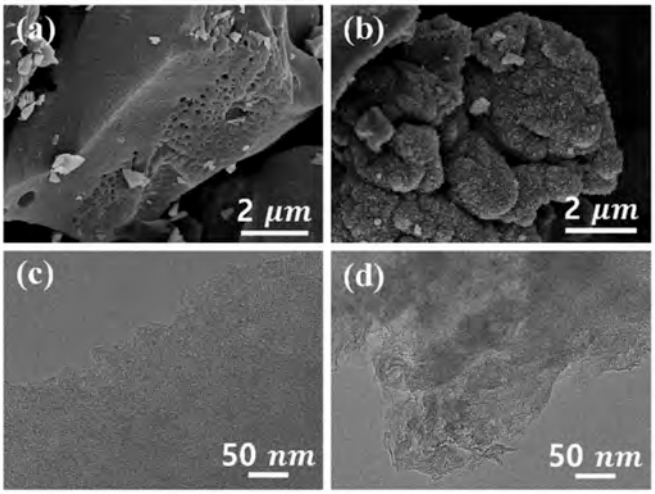

Fig. 8. SEM images show smooth surface of pristine catalyst (a) and surface roughening of used catalyst (b) due to carbon deposition. TEM images reveal the emergence of a wrinkled-graphene layer after 24 h of methane decomposition (d) compared to the pristine surface (c). Reproduced with permission from reference [124]. Copyright 2023 SpringerNature.

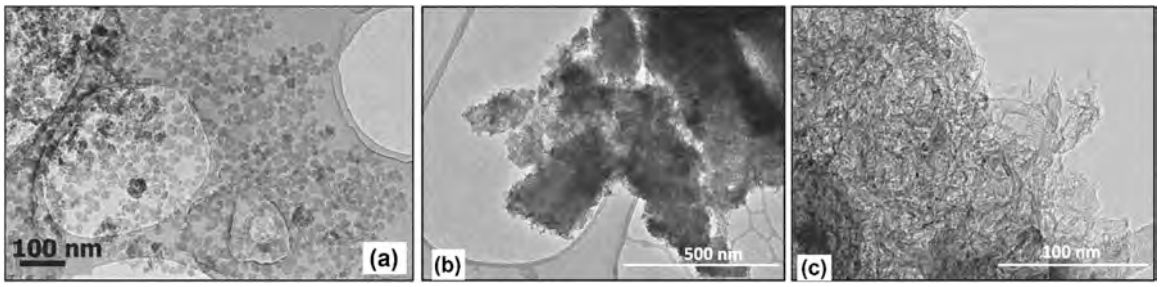

Fig. 9. RH-SiO_2 as a catalyst for the decomposition of methane for H_2 production. TEM images of the pristine (a) and used (b,c) states of RH-SiO_2 catalyst. The carbon structures grew towards the outer part of the silica nanoparticles so that the carbon deposition did not cause negative impacts on the catalytic activity of RH-SiO_2. Reproduced with permission from reference [17]. Copyright 2021 Elsevier.

catalytic activity compared to the Ni@α-Al_2O_3 catalyst synthesized under similar routes using commercial α-Al_2O_3 as a common support material [126]. Guo et al. applied the direct impregnation method to synthesize Cu@RH-SiO_2 catalyst using $ZnCl_2$ as an additional activation agent during the thermal treatment of RH [127]. They used the obtained Cu@RH-SiO_2 catalyst for the cracking of biomass to produce hydrogen-carrying syngas and reported a high biomass conversion efficiency of 94.5 %, attesting the remarkable catalytic activity of the catalyst [127]. Dong et al. reported the synthesis of Ni@RH-SiO_2 with an Ni loading of 10.42 wt% and the subsequent use of this catalyst coupled with microwave in the biomass pyrolysis for syngas production [128]. They indicated that Ni@RH-SiO_2 coupled with microwave exhibited a high catalytic effect and enabled the maximum biomass conversion efficiency of 97.3 %, corresponding to the CO and H_2 yields of 274.0 ml/g and 248.9 ml/g, respectively, at the reaction temperature of 700 °C [128]. These findings attested the benefits of combining catalysts and microwave in promoting the biomass decomposition.

Steam reforming reactions. Guo et al. synthesized a Ni@RH-SiO_2 catalyst and indicated that this catalyst worked well for the acetic acid steam reforming reactions, in which, the carbon conversion reached 95.3 % and the H2 yield achieved at 2.38 mol/mol when the reforming was conducted at 700 °C [129]. Suriya et al. reported the synthesis of Ni@RH-SiC for steam reforming of fusel oil (i.e. mixed alcohols resulting from ethanol production) for the hydrogen generation. RH-SiC was derived from pyrolysis of RH at high temperatures (1300, 1500, and 1700 °C). Ni nanoparticles were then embedded onto the RH-SiC surface to yield Ni@RH-SiC. The most effective Ni@RH-SiC was obtained when RH was pyrolysed at 1500 °C due to the formation of a rod structure and β-SiC phase with the highest surface area (64 m^2/g), much higher than that of SiC pyrolysed at 1300 °C (19 m^2/g) and 1700 °C (25 m^2/g). The best obtained Ni@RH-SiC delivered the highest catalytic activity with a hydrogen yield of 29 % after 180 min and with no considerable loss in activity over 300 min [130].

RH as a feedstock for hydrogen generation. We have attested the great potential of RH for the synthesis of hydrocarbon decomposition catalysts where the RH-derived materials are used as catalysts for hydrogen generation. Certainly, RH itself is an abundant biomass so it can also serve as a direct feedstock for hydrogen generation where RH is decomposed to yield hydrogen. Zeng et al. reported the production of hydrogen-rich gas via steam gasification of RH followed by catalytic reforming of the resulting syngas using CeO_2@Ni-CaO bifunctional catalysts [131]. Under the experiment conditions of 500 °C, steam/-carbon molar ratio of 5 and catalyst/RH mass ratio of 2.5, the authors obtained a RH-derived fuel gas mixture with hydrogen concentration of 85.81 vol% and hydrogen yield of 35.82 mmol per g of RH [131]. Qi et al. employed one-step in-situ catalytic pyrolysis of RH at 500 °C to produce hydrogen-rich syngas, phenol-rich bio-oil and nanostructured porous carbons [132]. They indicated that molten potassium salts and water vapor aided the creation of porous carbon with high graphitisation degrees and rich pore structures coupled with the generation of more hydrogen [132]. Representative studies of repurposing RH for hydrogen production are tabulated in Table 4.

6. Drug carriers

Owing to the intrinsic advantages such as having biogenic nature, high-purity and tunable structures, RH-silica possesses substantial potential for drug loading and carrier toward the controlled release in medical applications [21]. This novel prospect has sparked an emerging direction of developing biogenic RH-SiO_2 for medical and biotech applications. Dhinasekaran et al. fabricated nano-RH-SiO_2 for applications as a chemotherapeutic agent (Fig. 10) [133]. They obtained two types of RH-SiO_2 particles with mean sizes at ~20 nm and ~40 nm, respectively. These materials were loaded with 5-Fluorouracil by either direct conjugation or chitosan mediated conjugation. The smaller particles (i.e. ~20 nm) showed a better drug loading capacity and the chitosan mediated conjugation of drug exhibited a sustained release in acidic pH [133]. Also, the toxicity studies indicated that the chitosan mediated drug conjugation on the RH-SiO_2 displayed lesser toxic to fibroblast cell lines and higher toxicity towards cancer cell lines, in comparison with the direct conjugation. These results indicated the suitability of RH-SiO_2 for cancer cell-targeted delivery [133]. Chen et al. fabricated mesoporous RH-SiO_2 nanoparticles as effective carriers for cancer drug delivery [134]. They showed that the obtained RH-SiO_2 exhibited high biocompatibility, large surface area and porous structure as mesoporous nanoparticles for excellent drug carriers. The usage of these mesoporous nanoparticles was tailored by incorporating lanthanides europium and gadolinium into the RH-SiO_2 surface to make them fluorescent and magnetically active for the purpose of detection and tracking under confocal fluorescence microscopy and magnetic resonance imaging [134]. The conjugation of folic acid and aptamer AS1411 on the mesoporous RH-SiO_2 nanoparticles showed enhancement in targeting cancer cells, attesting the promising capability of delivering clinical drugs to specific aberrant tissues with a dual function as targeting and imaging for enhanced cancer therapy [134]. Soundharraj et al. compared RH-SiO_2 nanoparticles with the silica synthesized using organic precursor (TEOS) via sol-gel precipitation (called TEOS-SiO_2) [135]. Both silica samples were then functionalised with protoporphyrin (PpIX, an efficient photosensitiser) to assess the photodynamic therapy against target tumor cells [135]. The drug loading capacity, assessed based on 5-Fluorouracil conjugation on each type of the silica, indicated that the functionalized silica was suitable for combined therapeutic and diagnostic in biomedical practices, yet RH-SiO_2 outperformed TEOS-SiO_2 in terms of biocompatibility against blood cells. This study further attested the benefit of the biogenic nature of RH-SiO_2 for medical applications [135]. Andrade et al. evaluated the capacity of mesoporous RH-SiO_2 nanoparticles for loading and release the doxorubicin (DOX) chemotherapeutic drug [136]. They showed attractive textural characteristics and colloidal stability of the mesoporous RH-SiO_2 nanoparticles, and attributed these properties to a high efficiency of DOX loading [136]. They also indicated that the DOX@RH-SiO_2 were not cytotoxic for healthy fibroblast cells, but killed about 70 % of colorectal cancer cells

Table 4
RH-derived materials for applications in hydrogen generation.

Catalysts(*)	Reactions and notes	Source
Metal@RH-SiO_2 (Catalyst)	Methane decomposition: RH-SiO_2 with larger surface area and amorphous structure displayed the highest catalytic activity. Acid-leached RH-SiO_2 showed a remarkable resistance against deactivation.	Gómez-Pozuelo et al. [17]
RH-SiO_2 versus Ni@RH-SiO_2 (Catalyst)	Methane decomposition: RH-SiO_2 without nickel showed moderate activity with the CH_4 conversion up to 38.83 %. Ni@RH-SiO_2 showed high activity with a CH_4 conversion of 74.33 %.	Zhao et al. [125]
Ni@RH-SiO_2 versus Ni@α-Al_2O_3 (Catalysts)	Steam gasification: Ni@RH-SiO_2 enabled a maximum H_2 generation of 0.471 mol/(g feedstock × g catalyst). Ni@RH-SiO_2 showed better activity than the standard Ni@α-Al_2O_3 catalyst.	Farooq et al. [126]
Cu@RH-SiO_2 (Catalyst)	Cracking biomass for H_2: The catalyst showed a biomass conversion efficiency of 94.5 %, attesting its high catalytic activity.	Guo et al. [127]
Ni@RH-SiO_2 coupled with microwave (Catalyst)	Biomass pyrolysis for syngas: Ni@RH-SiO_2 coupled with microwave enabled a maximum biomass conversion of 97.3 %, giving the CO and H_2 yields of 274.0 ml/g and 248.9 ml/g, respectively, at 700 °C. These findings attested the benefits of combining catalysts and microwave in promoting the biomass decomposition.	Dong et al. [128]
Ni@RH-SiO_2 (Catalyst)	Steam reforming for H_2: Carbon conversion reached 95.3 % and H_2 yield reached 2.38 mol/mol when reforming at 700 °C.	Guo et al. [129]
Ni@RH-SiC (Catalyst)	Steam reforming of fusel oil (i.e. mixed alcohols resulting from ethanol production) for the H_2 generation. RH pyrolysis at 1300, 1500, and 1700 °C yielded SiC. Incorporating Ni nanoparticles onto the RH-SiC surface yielded Ni@RH-SiC. Pyrolysis at 1500 °C yielded the best Ni@RH-SiC with a rod structure and β-SiC phase and high surface area (64 m^2/g), which showed high catalytic activity with a H_2 yield of 29 % after 180 min and with no considerable loss in activity over 300 min.	Suriya et al. [130]
RH (Feedstock)	Production of H_2-rich gas via steam gasification of RH followed by catalytic reforming of the resulting syngas using CeO_2@Ni-CaO catalysts. After catalytic reforming, a fuel gas mixture with H_2 concentration of 85.81 vol%. The H_2 yield was 35.82 mmol per g of RH.	Zeng et al. [131]
RH (Feedstock)	One-step in-situ catalytic pyrolysis of RH at 500 °C to produce H_2-rich syngas, phenol-rich bio-oil and nanostructured porous carbons. Molten potassium salts and water vapor aided the creation of porous carbon with high graphitisation and rich pore structures coupled with generation of more H_2.	Qi et al. [132]

after 72 h, demonstrating the promising applications as targeted cancer therapy [136].

7. Other applications

In addition to the emerging directions discussed in previous sections, RH-derived materials also show unique potential for applications in many other sectors, including the followings.

Pure silicon: Ultrapure silicon plays a pivotal role in the high-tech industry. High-tech applications require extremely pure silicon, with a purity grade over 99.99999 % (seven digits) for electronics applications and over 99.9999 % (six digits) for solar applications [137–139]. Although silicon is the second most abundant element on Earth, the extraction and purification of Earth-sourced silicon involve highly energy-intensive metallurgical processes, which leads to high economic and environmental costs. It is expected that RH-bound biogenic silicon with the inherent high reactivity presents a promising source of high-quality silicon for high-tech applications [140]. Barati et al. filed a worldwide patent for the production of solar grade silicon from RH-SiO_2 [23]. Marchal et al. reported a simplified, efficient and low-carbon-footprint method for producing solar grade silicon from RH [141]. First, the RHA was purified using acid milling coupled with boiling-water washing. Then, the purified RHA was pelletised for subsequent carbothermal reduction in a 50 kW electric arc furnace (EAF) at 1700–2100 °C in batch mode [141]. They claimed the acquisition of silicon purity 99.9999 wt% (six digits) with B contents of ≈ 0.1 ppm by weight [141].

Supercapacitors: Supercapacitors open a new pathway for energy storage and are expected to play increasing roles in the era of energy transition. RH-derived nano-hybrids emerged as promising efficient low-cost materials for supercapacitors. Vijayan et al. synthesized tin oxide-decorated amorphous silica (SnO_2@RH-SiO_2) via microwave combustion route as a material for supercapacitors [22]. The SnO_2@RH-SiO_2 displayed a nano-hybrid containing SnO_2 with rutile tetragonal crystalline structure embedded in the amorphous RH-SiO_2 [22]. The SnO_2@RH-SiO_2 showed a specific capacitance of 448, 330, 275, 240, 225 and 200 F/g corresponding to the current density of 1, 2, 4, 6, 8 and 10 A/g, respectively. The inclusion of SnO_2 nanocrystals on RH-SiO_2 created surface reactivity for charging and discharge, which ultimately enhanced the charge storage capacity [22]. Priyan et al. synthesized nickel oxide-decorated RH-SiO_2 (NiO@RH-SiO_2) via a microwave-assisted sol-gel process [142]. The undecorated RH-SiO_2 showed a limited specific capacitance of 102 F/g while the best-obtained NiO@RH-SiO_2 showed a much higher value of 506 F/g under the same current density of 0.5 A/g [142]. The NiO@RH-SiO_2 electrode displayed an excellent energy density of 31.25 Wh kg−1 at a power density of 745 W kg−1 and long-term cyclic stability, showing only 3.6 % loss of capacitance over 10,000 cycles [142].

Quantum dots: Biogenic structure-tunable RH-SiO_2 showed promising precursor for fabrication of quantum dots (QDs). For example, Astuti et al. fabricated RH-derived silica quantum dots (Si-QDs) and obtained the material with particle sizes between 0.386 and 2.5 nm that adsorbed light with the peak wavelength of about 250–400 nm and emitted a purplish-blue colour [24]. The Si-QDs had a band gap of 1.59–2.36 eV and HOMO-LUMO of 127 99.5 kcal/mol. The SiO_2 content was of the Si-QDs was 97 % and the balance was impurity such as K, Fe, and Ca [24]. The obtained energy gap 1.59–2.36 eV and HOMO-LUMO 127 99.5 kcal/mol. The smaller size of Si-QDs led to a higher band gap as a result of the quantum confinement effect [24]. Wang et al. synthesized graphene quantum dots (G-QDs) with a mean size of 3.9 nm using RH as the feedstock [143]. The obtained G-QDs emitted bright blue photoluminescence under 365 nm ultraviolet irradiation and showed well-dispersed property in water (Fig. 11) [143]. The G-QDs showed high sensitivity and selectivity toward Fe^{3+} ions, attesting the potential applications as Fe^{3+} sensing [143]. In addition, it was found that the

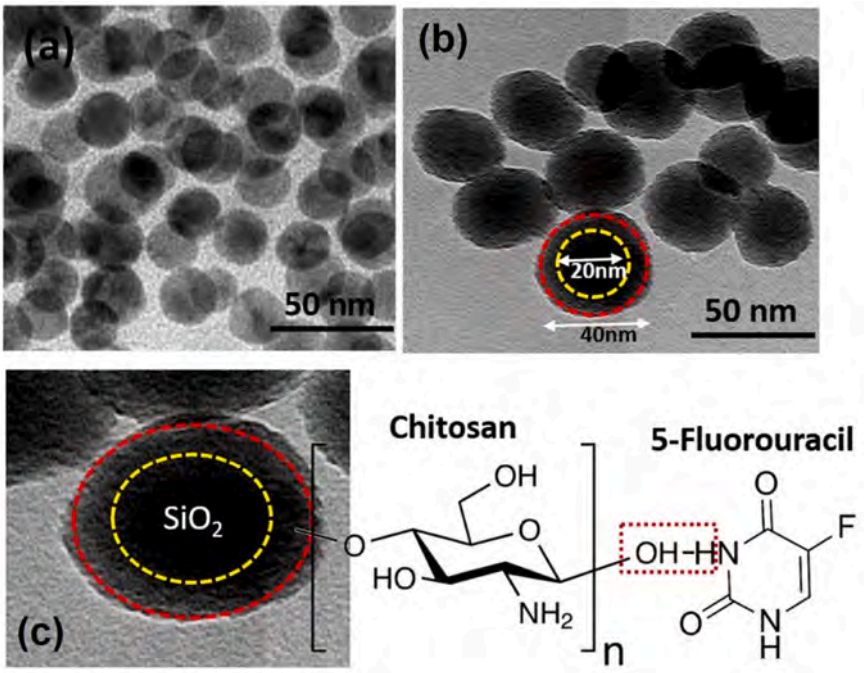

Fig. 10. TEM images of as-prepared RH-SiO_2 nanoparticles (a) and these RH-SiO_2 particles after being coated with chitosan and loaded with 5-Fluorouracil (b). The image (c) shows an illustration of the binding between 5-Fluorouracil and chitosan supported on the RH-SiO_2 nanoparticles. Reproduced with permission from reference [133]. Copyright 2020 Elsevier.

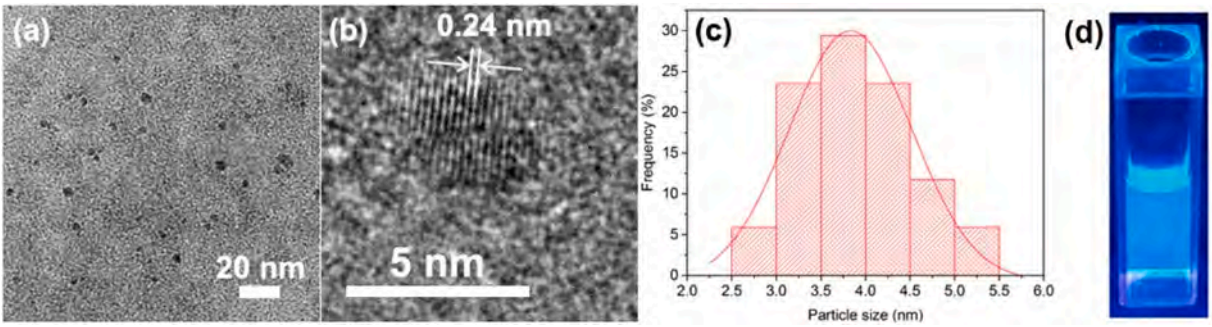

Fig. 11. (a) TEM and (b) high-resolution TEM image of graphene quantum dots (G-QDs). The size distribution (c) and the dispersion and glowing under 365 nm UV light irradiation (d) of the G-QDs. Reproduced with permission from reference [143]. Copyright 2018 American Chemical Society.

G-QDs were very biocompatible and, thus, suitable for utilisation in cell imaging in biomedical applications [144,145]. Wei et al. used high-purity amorphous RH-SiO_2 to prepare green phosphor (Mn-doped zinc silicate, $Zn_2SiO_4 : Mn^{2+}$) [146]. They showed that the RH-derived $Zn_2SiO_4 : Mn^{2+}$ outperformed the counterpart synthesized using commercial silica with respect to the photoluminescence intensity and quantum yield, demonstrating the great potential of RH-derived phosphor as an cost-effective alternative to commercial products [146].

8. Outlooks

Vibrant research growth is envisaged for this particular field. Future advances shall deliver innovations to enable fabricating RH-derived functional materials with tailored properties while improving the cost-efficacy and mitigating the environmental footprints of the process. This goal can be achieved through focusing the research in four strategic pillars, namely (1) complete utilisation of RH, (2) shifting toward eco-friendly reagents, (3) exploiting the synergistic effect of microwave/ultrasound and chemicals for enhancing the conversion and (4) developing enzymatic processing of RH (Fig. 12).

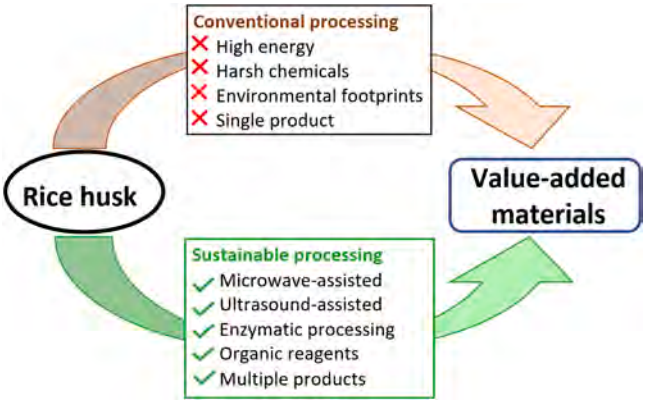

Fig. 12. Prospect for more sustainable approaches for processing of RH.

Complete utilisation of RH for multiple products: In most previous studies, a single product was obtained from the processing of RH. This single product was either amorphous silica, activated carbon, SiC

hybrid materials, etc (as discussed in previous sections). In such conventional processes, RH was utilised in part as the other components were not recovered. For example, the extraction of silica from RH via calcination-based decarbonation entails two major issues considering the economic and environmental aspects. First, decarbonation of RH via calcination results in significant emission of carbon dioxide and does not align with the global roadmap toward net-zero emissions. Furthermore, valuable carbonaceous components such as cellulose and lignin are not recovered. Hence, complete utilisation of RH is necessary to recover both the silicon (or silica) and carbonaceous materials from RH for maximising the economic values and mitigating the environmental footprints of the process. In particular, the by-products of the pyrolysis of RH (e.g., bio-gas and bio-oil) should be also recovered to enhance the profitability and reduce the environmental impacts of the process. This new direction toward the complete utilisation of RH to obtain both silica and carbonaceous materials has been considered by several recent studies with promising results [38–40, 144, 145] and, therefore, should be focused in the future studies.

Shifting toward eco-friendly reagents: The majority of previous works used harmful and expensive inorganic reagents (e.g., hydrochloric acid, nitric acid, sodium hydroxide, zinc chloride, etc.) for the treatment of RH. Inorganic reagents generally show superior performances in RH processing compared to organic reagents [33]. However, the use of inorganic reagents leads to significant environmental footprints considering the way they are produced and the treatment of spent solutions. First, inorganic reagents are often produced through energy-intensive and chemicals-intensive processes that create harmful impacts on the environments. Secondly, the spent inorganic reagents are usually hazardous liquid wastes that are harmful and expensive for the subsequent treatments. These pronounced drawbacks of inorganic reagents have driven efforts to find alternative solutions.

It is noted that there has been an interest in using physical activation agents such as CO_2 and steam in the RH treatments. These physical activation agents can be more environmentally benign than the chemical counterparts such as KOH and $SnCl_2$ in some particular applications, for example, in the production of activated carbon from RH [147–150]. Even so, in many cases, chemical reagents are required for the extraction and separation of components in the RH. For example, physical processes based on steam or CO_2 activation are unable to remove alkaline elements and other impurities from the RH biochar for producing high-purity RH-derived silica or carbon-based products [147,150]. Hence, chemical processes are still required for repurposing RH for achieving more controllable product quality [150]. Future studies shall look for more sustainable chemicals to replace the harsh ones that are currently used as well as developing more efficient processes that enable better recycling of the used reagents.

A number of researchers have attempted to switch to more environmentally friendly organic reagents such as acetic acid, humic acid, fulvic acid, gluconic acid, etc. The challenge for using eco-friendly reagents is that they are not as effective as the inorganic counterparts [33]. Even though, there have been a few studies claimed the success in replacing inorganic reagents by eco-friendly alternatives [36,151,152]. Hence, finding and switching to eco-friendly reagents for the RH treatment would be an integral part of the future research.

Microwave or ultrasound-assisted conversion: Incorporating external energy in the form of microwave or ultrasound presents a strategy for sustainable processing of RH by exploiting the synergy between the applied energy and chemicals to facilitate the bond breakage and accelerate the extraction of target components from RH. In particular, microwave-assisted extraction and ultrasound-assisted extraction are two most popular and effective techniques in biorefinery [153–157]. The aid of external energy supply can foster the biomass conversion so that the usage of expensive can be minimised, which ultimately mitigates the overall environmental footprints of the process. In addition, external energy like microwave might exhibit selective effects towards certain components and bonds, thereby, improving the purity of the extracted products. Hence, incorporating external energy to aid the chemical process would present a strategic development in this field.

Enzymatic processing: Works reported in the literature are based primarily on chemical and thermal processes for the treatment of RH which are both energy-intensive and chemicals-intensive. Meanwhile, there is emerging direction in developing enzymatic hydrolysis of biomass [158,159]. Enzymatic hydrolysis of biomass in general and RH in particular presents a big scope of research lying ahead considering the development and selection of appropriate types of enzymes as well as optimisation of the working conditions to achieve the best outcomes in terms of economic and environmental benefits [160].

Challenges for upscaling and commercialisation: While the potential applications of RH-derived materials are vast, the transition from laboratory-scale processes to large-scale production requires overcoming significant hurdles. The silica content in RH varies significantly depending on the rice variety and cultivation conditions, typically ranging from 13 % to 29 % by weight [161], which can lead to inconsistent quality of final products, making it difficult to meet the stringent specifications required for commercial applications. The optimisation of the processing conditions for the conversion of RH into silica and carbon needs more attention. The combustion temperature, for instance, plays a crucial role in determining the structural properties of the resulting silica. Higher temperatures can lead to the formation of crystalline silica, which has a lower surface area and porosity compared to amorphous silica [162]. Novel reactor designs will play an integral role in the upscaled experiments for improving the conversion rate and efficiency as well as energy-savings [163]. This necessitates careful control of the combustion process to ensure that the desired properties of the silica are achieved. Economic factors also pose significant barriers to the commercialisation of RH-derived products. The initial investment required for setting up processing facilities can be substantial, particularly for smallholder farmers or small enterprises. The costs associated with the transportation, storage, and processing of rice husk can further reduce the economic viability of these ventures [164]. In addition, the market for silica and carbon products derived from RH is still developing, and establishing a reliable customer base may take time and effort. The competition from established silica and carbon suppliers can also hinder the entry of new players into the market. The regulatory landscape surrounding the use of agricultural waste for industrial applications can be complex. Compliance with environmental regulations regarding emissions from burning rice husk and the disposal of by-products such as rice husk ash (RHA) can impose additional costs and operational constraints. The potential for environmental pollution from improper handling of these materials must be addressed to gain public acceptance and regulatory approval for large-scale operations.

9. Conclusion

With the intrinsic advantages considering the abundant quantity and exceptional quality, RH is a precious resource for the synthesis of advanced functional materials in the context of low-carbon circular economies. The most unique value of RH is the inherent hybrid nature of the naturally-blended carbon/silicon complexes, which enables the production of nanostructured hybrid materials with tailored properties, those are otherwise not possible to obtain via synthetic means. Repurposing RH toward value-added materials presents a vibrant research field with a clear prospect of further success in the future. This paper presents an inspiring contribution to promote the ongoing studies in agrowaste recycling toward a circular decarbonised world.

CRediT authorship contribution statement

Anh Nguyen: Writing – review & editing, Visualization, Validation, Methodology, Conceptualization. **Muxina Konarova:** Writing – review & editing, Visualization, Validation, Methodology, Conceptualization. **Ngoc Nguyen:** Writing – original draft, Visualization, Validation,

Methodology, Funding acquisition, Formal analysis, Conceptualization.

Declaration of Competing Interest

The authors declare that they have no known competing financial interests or personal relationships that could have appeared to influence the work reported in this paper.

Acknowledgements

Ngoc N. Nguyen gratefully acknowledges the Australian Research Council (ARC) for the funding support through the Discovery Early-Career Researcher Awards (DECRA, DE240100722).

Data Availability

Data will be made available on request.

References

[1] Y. Wang, J.J. Wu, Thermochemical conversion of biomass: potential future prospects, Renew. Sustain. Energy Rev. 187 (2023) 113754.
[2] J. Sherwood, The significance of biomass in a circular economy, Bioresour. Technol. 300 (2020) 122755.
[3] M. Kordi, N. Farrokhi, M.I. Pech-Canul, A. Ahmadikhah, Rice husk at a glance: from agro-industrial to modern applications, Rice Sci. 31 (1) (2024) 14–32.
[4] Shahbandeh, M. World Production Volume of Milled Rice from 2008/2009 to 2023/24. 2024 [cited 2025; Available from: ⟨https://www.statista.com/statistics/271972/world-husked-rice-production-volume-since-2008/⟩.
[5] E. Omrani, P.L. Menezes, P.K. Rohatgi, State of the art on tribological behavior of polymer matrix composites reinforced with natural fibers in the green materials world, Eng. Sci. Technol. Int. J. 19 (2) (2016) 717–736.
[6] R. Pode, B. Diouf, G. Pode, Sustainable rural electrification using rice husk biomass energy: a case study of Cambodia, Rnewable Sustain. Energy Rev. 44 (2015) 530–542.
[7] B. Singh, 13 - Rice husk ash, in: R. Siddique, P. Cachim (Eds.), in *Waste and Supplementary Cementitious Materials in Concrete*, Woodhead Publishing, 2018, pp. 417–460.
[8] M.N. Al-Khalaf, H.A. Yousif, Use of rice husk ash in concrete, Int. J. Cem. Compos. Lightweight Concr. 6 (4) (1984) 241–248.
[9] A. Siddika, M.A.A. Mamun, R. Alyousef, H. Mohammadhosseini, State-of-the-art review on rice husk ash: a supplementary cementitious material in concrete, J. King Saud. Univ. Eng. Sci. 33 (5) (2021) 294–307.
[10] N.N. Ngoc, L.X. Thanh, L.T. Vinh, B.T. Van Anh, High-purity amorphous silica from rice husk: preparation and characterization, Vietnam J. Chem. 56 (6) (2018) 730–736.
[11] A.V. Fafure, D.B. Bem, S.W. Kahuthu, A.A. Adediran, M.O. Bodunrin, A. A. Fabuyide, C. Ajanaku, Advances in silicon–carbon composites anodes derived from agro wastes for applications in lithium-ion battery: a review, Heliyon 10 (11) (2024).
[12] M. Muraleedharan Pillai, N. Kalidas, X. Zhao, V.P. Lehto, Biomass-based silicon and carbon for lithium-ion battery anodes, Front. Chem. 10 (2022).
[13] S.K. Singh, S. Raj, D. Debasish, Preparation of SiC from rice husk: past, present, and future, *Lect. Notes Mech. Eng.* (2023).
[14] C. Padwal, H.D. Pham, L.T.M. Hoang, S. Mundree, D. Dubal, Deep eutectic solvents assisted biomass pre-treatment to derive sustainable anode materials for lithium-ion batteries, Sustain. Mater. Technol. 35 (2023) e00547.
[15] G.S. dos Reis, P. Molaiyan, C.M. Subramaniyam, F. García-Alvarado, A. Paolella, H.P. de Oliveira, U. Lassi, Biomass-derived carbon–silicon composites (C@Si) as anodes for lithium-ion and sodium-ion batteries: a promising strategy towards long-term cycling stability: a mini review, Electrochem. Commun. 153 (2023) 107536.
[16] Y. Li, J.Y. Lan, J. Liu, J. Yu, Z. Luo, W. Wang, L. Sun, Synthesis of gold nanoparticles on rice husk silica for catalysis applications, Ind. Eng. Chem. Res. 54 (21) (2015) 5656–5663.
[17] G. Gómez-Pozuelo, P. Pizarro, J.A. Botas, D.P. Serrano, Hydrogen production by catalytic methane decomposition over rice husk derived silica, Fuel 306 (2021).
[18] Y. Shen, K. Yoshikawa, Tar conversion and vapor upgrading via in situ catalysis using silica-based nickel nanoparticles embedded in rice husk char for biomass pyrolysis/gasification, Ind. Eng. Chem. Res. 53 (27) (2014) 10929–10942.
[19] H. Ouyang, N. Safaeipour, R.S. Othman, M. Otadi, R. Sheibani, F. Kargaran, Q. Van Le, H.A. Khonakdar, C. Li, Agricultural waste-derived (nano)materials for water and wastewater treatment: current challenges and future perspectives, J. Clean. Prod. 421 (2023) 138524.
[20] A.K. Badawi, K. Kriaa, R.M. Osman, R. Hassan, Modified rice husk waste-based filter for wastewater treatment: pilot study and reuse potential, Chem. Eng. Technol. 47 (7) (2024) 968–975.
[21] G. Smagulova, A. Imash, A. Baltabay, B. Kaidar, Z. Mansurov, Rice-husk-based materials for biotechnological and medical applications, C. -J. Carbon Res. 8 (4) (2022).
[22] R. Vijayan, G.S. Kumar, G. Karunakaran, N. Surumbarkuzhali, S. Prabhu, R. Ramesh, Microwave combustion synthesis of tTin oxide-decorated silica nanostructure using rice husk template for supercapacitor applications, J. Mater. Sci.: Mater. Electron. 31 (7) (2020) 5738–5745.
[23] M. Barati, K.K. Larbi, R. Roy, V.I. Lakshmanan, R. Sridhar, Production of high purity silicon from amorphous silica, Process Res. Ortech Inc: Can. (2010) 1–26.
[24] E.S. Astuti, A.A. Sonief, M. Sarosa, N. Ngafwan, I.N.G. Wardana, Synthesis, characterization and energy gap of silica quantum dots from rice husk, Bioresour. Technol. Rep. 20 (2022).
[25] S.S. Hossain, L. Mathur, P.K. Roy, Rice husk/rice husk ash as an alternative source of silica in ceramics: a review, J. Asian Ceram. Soc. 6 (4) (2018) 299–313.
[26] M. Ahmaruzzaman, V.K. Gupta, Rice husk and its ash as low-cost adsorbents in water and wastewater treatment, Ind. Eng. Chem. Res. 50 (24) (2011) 13589–13613.
[27] B.A. Tayeh, R. Alyousef, H. Alabduljabbar, A. Alaskar, Recycling of rice husk waste for a sustainable concrete: a critical review, J. Clean. Prod. 312 (2021) 127734.
[28] Y. Shen, Rice Husk silica-derived nanomaterials for battery applications: a literature review, J. Agric. Food Chem. 65 (5) (2017) 995–1004.
[29] R.A. Bakar, R. Yahya, S.N. Gan, Production of high purity amorphous silica from rice husk, Procedia Chem. 19 (2016) 189–195.
[30] M.I.I.R. Source, Silica Mark. Size Share Anal. - Growth Trends Forecasts (2024 - 2029) (2024). ⟨https://www.mordorintelligence.com/industry-reports/silica-market⟩, 19/07/2024]; Available from.
[31] J.H. Lee, J.H. Kwon, J.-W. Lee, H.-s Lee, J.H. Chang, B.-I. Sang, Preparation of high purity silica originated from rice husks by chemically removing metallic impurities, J. Ind. Eng. Chem. 50 (2017) 79–85.
[32] S. Sankar, N. Kaur, S. Lee, D.Y. Kim, Rapid sonochemical synthesis of spherical silica nanoparticles derived from brown rice husk, Ceram. Int. 44 (7) (2018) 8720–8724.
[33] D. Dhaneswara, J.F. Fatriansyah, F.W. Situmorang, A.N. Haqoh, Synthesis of amorphous silica from rice husk ash: comparing HCl and CH3COOH acidification methods and various alkaline concentrations, Int. J. Technol. 11 (1) (2020) 200–208.
[34] J.Y. Park, W. Mun, J. Chun, B.I. Sang, R.J. Mitchell, J.H. Lee, Alkali extraction to detoxify rice husk-derived silica and increase its biocompatibility, ACS Sustain. Chem. Eng. 10 (24) (2022) 7811–7817.
[35] J. Chun, Y.Mo Gu, J. Hwang, K.K. Oh, J.H. Lee, Synthesis of ordered mesoporous silica with various pore structures using high-purity silica extracted from rice husk, J. Ind. Eng. Chem. 81 (2020) 135–143.
[36] S. Kim, J.Y. Park, Y.M. Gu, I.S. Jang, H. Park, K.K. Oh, J.H. Lee, J. Chun, Eco-friendly and facile synthesis of size-controlled spherical silica particles from rice husk, Nanoscale Adv. 3 (24) (2021) 6965–6973.
[37] K. Kordatos, S. Gavela, A. Ntziouni, K.N. Pistiolas, A. Kyritsi, V. Kasselouri-Rigopoulou, Synthesis of highly siliceous ZSM-5 zeolite using silica from rice husk ash, Microporous Mesoporous Mater. 115 (1-2) (2008) 189–196.
[38] H.J. Jung, H. Kwak, J. Chun, K.K. Oh, Alkaline fractionation and subsequent production of nano-structured silica and cellulose nano-fibrils for the comprehensive utilization of rice husk, Sustainability 13 (4) (2021) 1–18.
[39] N.T. Nguyen, N.T. Tran, T.P. Phan, A.T. Nguyen, M.X.T. Nguyen, N.N. Nguyen, Y. H. Ko, D.H. Nguyen, T.T.T. Van, D. Hoang, The extraction of lignocelluloses and silica from rice husk using a single biorefinery process and their characteristics, J. Ind. Eng. Chem. 108 (2022) 150–158.
[40] Z. Wei, A.T. Smith, W.R.T. Tait, J. Liu, H. Ding, H. Wang, W. Wang, L. Sun, Lignocellulose aerogel and amorphous silica nanoparticles from rice husks, J. Leather Sci. Eng. 3 (1) (2021) 2.
[41] A.S. Aliyu, U.Sa Aliyu, A.M. Hamza, B.B. Nyakuma, M.S. Liman, U.I. Gaya, A. M. Dunama, J.D. Zira, M.M. Liman, Synthesis and characterisation of rice husk and palm fruit bunch silica: compositional, structural, and thermal analyses, Biomass-.-. Conv. Bioref. (2024).
[42] B.B. Nyakuma, S. Wong, G.R. Mong, L.N. Utume, O. Oladokun, K.Y. Wong, T.J. P. Ivase, T.A.T. Abdullah, Bibliometric analysis of the research landscape on rice husks gasification (1995–2019), Environ. Sci. Pollut. Res. 28 (36) (2021) 49467–49490.
[43] Y.M. Peralta, R. Molina, S. Moreno, Chemical and structural properties of silica obtained from rice husk and its potential as a catalytic support, J. Environ. Chem. Eng. 12 (2) (2024) 112370.
[44] J. Saddique, M. Wu, W. Ali, X. Xu, Z.-G. Jiang, L. Tong, H. Zheng, W. Hu, Opportunities and challenges of nano si/c composites in lithium ion battery: a mini review, J. Alloy. Compd. 978 (2024) 173507.
[45] S. Sekar, T.A. Ahmed, A.I. Inamdar, Y. Lee, H. Im, D. Kim, S. Lee, Activated carbon-decorated spherical silicon nanocrystal composites synchronously-derived from rice husks for anodic source of lithium-ion battery, Nanomaterials 9 (7) (2019).
[46] Q. Ma, Y. Dai, H. Wang, G. Ma, H. Guo, X. Zeng, N. Tu, X. Wu, M. Xiao, Directly conversion the biomass-waste to si/c composite anode materials for advanced lithium ion batteries, Chin. Chem. Lett. 32 (1) (2021) 5–8.
[47] J. Gao, L. Li, J. Liu, F. Liu, Y. Han, X. Zhu, K. Ma, Efficient production of nanoporous silicon carbide from rice husk at relatively low temperature, Mendeleev Commun. 31 (5) (2021) 715–717.
[48] Y. Li, L. Liu, X. Liu, Y. Feng, B. Xue, L. Yu, L. Ma, Y. Zhu, Y. Chao, X. Wang, Extracting Lignin-SiO2 composites from si-rich biomass to prepare si/c anode materials for lithium ions batteries, Mater. Chem. Phys. 262 (2021).
[49] N. Lin, T. Xu, Y. Han, K. Shen, Y. Zhu, Y. Qian, A Molten salt strategy for deriving a porous si@c nano-composite from si-rich biomass for high-performance Li-ion batteries, RSC Adv. 6 (83) (2016) 79890–79893.

[50] M.K. Majeed, A. Saleem, C. Wang, C. Song, J. Yang, Simplified synthesis of biomass-derived si/c composites as stable anode materials for lithium-ion batteries, Chem. - Eur. J. 26 (46) (2020) 10544–10549.

[51] Z. Zhao, M. Cai, H. Zhao, Q. Ma, H. Xie, P. Xing, Y.X. Zhuang, H. Yin, Zincothermic-Reduction-Enabled Harvesting of an Si/C Composite from Rice Husks for a Li-Ion Battery Anode, ACS Sustain. Chem. Eng. 10 (15) (2022) 5035–5042.

[52] Y.C. Zhang, Y. You, S. Xin, Y.X. Yin, J. Zhang, P. Wang, X.S. Zheng, F.F. Cao, Y. G. Guo, Rice husk-derived hierarchical silicon/nitrogen-doped carbon/carbon nanotube spheres as low-cost and high-capacity anodes for lithium-ion batteries, Nano Energy 25 (2016) 120–127.

[53] K. Yu, H. Zhang, H. Qi, X. Gao, J. Liang, C. Liang, Rice husk as the source of silicon/carbon anode material and stable electrochemical performance, ChemistrySelect 3 (19) (2018) 5439–5444.

[54] H. Chu, Q. Wu, J. Huang, Rice husk derived silicon/carbon and silica/carbon nanocomposites as anodic materials for lithium-ion batteries, Colloids Surf., A 558 (2018) 495–503.

[55] W. Tao, C. Xu, P. Gao, K. Zhang, X. Zhu, D. Wu, J. Chen, Synthesis of core–shell silicon–carbon nanocomposites via in-situ molten salt-based reduction of rice husks: a promising approach for the manufacture of lithium-ion battery anodes, J. Colloid Interface Sci. 669 (2024) 902–911.

[56] S.F. Liu, C.H. Kuo, C.C. Lin, H.Y. Lin, C.Z. Lu, J.W. Kang, G.T.K. Fey, H.Y. Chen, Biowaste-derived Si@SiOx/C anodes for sustainable lithium-ion batteries, Electrochim. Acta 403 (2022).

[57] M. Gautam, G.K. Mishra, M. Furquan, K. Bhawana, D. Kumar, S. Mitra, Design of low-stress robust silicon and silicon-carbide anode with high areal capacity and high energy density for next-generation lithium-ion batteries, Chem. Eng. J. 472 (2023).

[58] T. Autthawong, O. Namsar, A. Yu, T. Sarakonsri, Cost-effective production of SiO2/C and Si/C composites derived from rice husk for advanced lithium-ion battery anodes, J. Mater. Sci.: Mater. Electron. 31 (12) (2020) 9126–9132.

[59] L. Liao, T. Ma, Y. Xiao, M. Wang, Y. Gao, T. Fang, Enhanced reversibility and cyclic stability of biomass-derived silicon/carbon anode material for lithium-ion battery, J. Alloy. Compd. 873 (2021).

[60] J.H. Choi, H.K. Kim, E.M. Jin, M.W. Seo, J.S. Cho, R.V. Kumar, S.M. Jeong, Facile and scalable synthesis of silicon nanowires from waste rice husk silica by the molten salt process, J. Hazard. Mater. 399 (2020).

[61] M.L.G. Pereira, D.S.S. Figueira, B.R. Girolamo, F. Vernilli, Synthesis of silicon carbide from rice husk, Ceramica 66 (379) (2020) 256–261.

[62] F. Unglaube, C.R. Kreyenschulte, E. Mejía, Development and application of efficient ag-based hydrogenation catalysts prepared from rice husk waste, ChemCatChem 13 (11) (2021) 2583–2591.

[63] F. Unglaube, J. Schlapp, A. Quade, J. Schäfer, E. Mejía, Highly active heterogeneous hydrogenation catalysts prepared from cobalt complexes and rice husk waste, Catal. Sci. Technol. 12 (10) (2022) 3123–3136.

[64] F. Unglaube, H. Atia, S. Bartling, C.R. Kreyenschulte, E. Mejía, Hydrogenation of epoxides to anti-markovnikov alcohols over a nickel heterogenous catalyst prepared from biomass (rice) waste, Helv. Chim. Acta 106 (2) (2023) e202200167.

[65] N.N. Nguyen, A.V. Nguyen, Nanoreactors" for boosting gas hydrate formation toward energy storage applications, ACS Nano 16 (8) (2022) 11504–11515.

[66] Y. Shen, Rice husk silica derived nanomaterials for sustainable applications, Renew. Sustain. Energy Rev. 80 (2017) 453–466.

[67] J.D. Sinniah, W.Y. Wong, K.S. Loh, R.M. Yunus, Physicochemical characterization of amine-functionalized bio-nanosilica extracted from rice husk ash as a platinum support, Mater. Today.: Proc. 57 (2022) 1276–1281.

[68] J. Janaun, N.N. Safie, N.J. Siambun, Synthesis, characterization and catalytic activity of carbon-silica hybrid catalyst from rice straw, AIP Conf. Proc. 1 (2016) **1756**.

[69] A.M. Grimm, L.Y. Dorsch, G.H. Kloess, D. Enke, A. Roppertz, Transition metal promoted combustion of rice husk and rice straw towards an energy optimized synthesis of biogenic silica, Biomass-.-. Bioenergy 155 (2021).

[70] H. Wang, S. Zhu, Z. Dai, X. Li, T. Zhou, Selective synthesis of large diameter single-walled carbon nanotubes on rice husk-derived catalysts, J. Environ. Chem. Eng. 11 (2) (2023).

[71] M. Ghadermazi, S. Moradi, R. Mozafari, Rice Husk-SiO2 supported bimetallic fe-ni nanoparticles: as a new, powerful magnetic nanocomposite for the qqueous reduction of nitro compounds to amines, RSC Adv. 10 (55) (2020) 33389–33400.

[72] E. Ramya, A. Thirumurugan, V.S. Rapheal, K. Anand, CuO@SiO2 nanoparticles assisted photocatalytic degradation of 4-nitrophenol and their antimicrobial activity studies, Environ. Nanotechnol., Monit. Manag. 12 (2019) 100240.

[73] G.-H. Lai, B.-S. Huang, T.-I. Yang, M.-H. Tsai, Y.-C. Chou, Preparation of highly stable and recyclable au/electroactive polyamide composite catalyst for nitrophenol reduction, Polymer 213 (2021) 123200.

[74] N.K.R. Bogireddy, P. Sahare, U. Pal, S.F.O. Méndez, L.M. Gomez, V. Agarwal, Platinum nanoparticle-assembled porous biogenic silica 3d hybrid structures with outstanding 4-nitrophenol degradation performance, Chem. Eng. J. 388 (2020) 124237.

[75] A.T. Vu, T.N. Xuan, C.H. Lee, Preparation of Mesoporous Fe2O3·SiO2 Composite from rice husk as an efficient heterogeneous fenton-like catalyst for degradation of organic dyes, J. Water Proc. Eng. 28 (2019) 169–180.

[76] W. Wang, H. Chen, J. Fang, M. Lai, Large-scale preparation of rice-husk-derived mesoporous SiO2@TiO2 as efficient and promising photocatalysts for organic contaminants degradation, Appl. Surf. Sci. 467-468 (2019) 1187–1194.

[77] J.H. Advani, K. Ravi, D.R. Naikwadi, H.C. Bajaj, M.B. Gawande, A.V. Biradar, Bio-waste Chitosan-derived N-doped CNT-supported Ni nanoparticles for selective hydrogenation of nitroarenes, Dalton Trans. 49 (30) (2020) 10431–10440.

[78] V.R. Madduluri, K.K. Mandari, V. Velpula, M. Varkolu, S.R.R. Kamaraju, M. Kang, Rice husk-derived carbon-silica supported ni catalysts for selective hydrogenation of biomass-derived furfural and levulinic acid, Fuel 261 (2020).

[79] J. Balbuena, M. Cruz-Yusta, A. Pastor, L. Sánchez, α-Fe2O3/SiO2 composites for the enhanced photocatalytic no oxidation, J. Alloy. Compd. 735 (2018) 1553–1561.

[80] A. Pastor, J. Balbuena, M. Cruz-Yusta, I. Pavlovic, L. Sánchez, ZnO on Rice husk: a sustainable photocatalyst for urban air purification, Chem. Eng. J. 368 (2019) 659–667.

[81] M. Lolage, M.G. Chaskar, A. Ghosh, Sulfonic acid functionalized precipitated silica as efficient solid acid catalyst for acetylation reactions, Nanosci. Nanotechnol. –Asia 13 (1) (2023) 57–65.

[82] A. Zare, E. Izadi, Preparation of a novel nanocatalyst based on rice husk-derived nano-silica and its application for the synthesis of pyrano[2,3-d]pyrimidine-2,4-diones and pyrano[2,3-d]pyrimidine-4-one-2-thiones, Res. Chem. Intermed. 49 (7) (2023) 2919–2931.

[83] E. Elimbinzi, S.S. Nyandoro, E.B. Mubofu, J.C. Manayil, A.F. Lee, K. Wilson, Valorization of rice husk silica waste: organo-amine functionalized castor oil templated mesoporous silicas for biofuels synthesis, Microporous Mesoporous Mater. 294 (2020) 109868.

[84] N., L. Hakkim, L. Nebhani, Polymer grafting on nitrone functionalized green silica via "grafting from" and "grafting to" approaches through enhanced spin capturing polymerization and a 1,3-dipolar cycloaddition reaction, Polym. Chem. 14 (39) (2023) 4547–4559.

[85] M. Pandey, N. Tsunoji, Y. Kubota, M. Bandyopadhyay, Amine and sulfonic acid anchored porous silica as recyclable heterogeneous catalysts for ring-opening of oxiranes, ChemistrySelect 7 (30) (2022).

[86] S. Jamnongphol, A. Jaturapiree, K. Sukrat, T. Saowapark, E. Chaichana, B. Jongsomjit, Rice husk-derived silica as a support for zirconocene/mmao catalyst in ethylene polymerization, Waste Biomass-.-. Valoriz. 11 (2) (2020) 769–779.

[87] H. Jin, L. Zhou, G. Zha, P. Huang, F. Wang, S. Li, M. Jiang, C. Liu, The simple construction of rice-husk-derived carbon catalyst for oxygen reduction reaction by the synergism of iron and nitrogen co-doping, Sustain. Energy Fuels 7 (18) (2023) 4525–4532.

[88] R.S. Gama, I.C.A. Bolina, É .C. Cren, A.A. Mendes, A novel functionalized sio2-based support prepared from biomass waste for lipase adsorption, Mater. Chem. Phys. 234 (2019) 146–150.

[89] R.B. Salah, H. Mosbah, A. Fendri, A. Gargouri, Y. Gargouri, H. Mejdoub, Biochemical and molecular characterization of a lipase produced by rhizopus oryzae, FEMS Microbiol. Lett. 260 (2) (2006) 241–248.

[90] R. Naraian, R.L. Gautam, Chapter 6 - Penicillium Enzymes for the Saccharification of Lignocellulosic Feedstocks, in: V.K. Gupta, S. Rodriguez-Couto (Eds.), in *New and Future Developments in Microbial Biotechnology and Bioengineering*, Elsevier: Amsterdam, 2018, pp. 121–136.

[91] P. Nikam, Y.S. Rajput, R. Sharma, S. Ranvir, Chapter 1 - Milk enzymes, in: Y. S. Rajput, R. Sharma (Eds.), in *Enzymes Beyond Traditional Applications in Dairy Science and Technology*, Academic Press, 2023, pp. 3–35.

[92] M.T. Morrissey, T. Okada, 17 - Marine Enzymes from Seafood By-products, in: F. Shahidi (Ed.), in *Maximising the Value of Marine By-Products*, Woodhead Publishing, 2007, pp. 374–396.

[93] N.B. Machado, G.J. Sabi, D.B. Hirata, A.A. Mendes, Enzymatic production of wax esters by esterification using lipase immobilized via physical adsorption on functionalized rice husk silica as biocatalyst, Biotechnol. Appl. Biochem. 70 (3) (2023) 1291–1301.

[94] G.J. Sabi, R.S. Gama, R. Fernandez-Lafuente, J. Cancino-Bernardi, A.A. Mendes, Decyl esters production from soybean-based oils catalyzed by lipase immobilized on differently functionalized rice husk silica and their characterization as potential biolubricants, Enzym. Microb. Technol. 157 (2022).

[95] N. Mori, H. Kawasaki, E. Nishida, Y. Kanemoto, H. Miyaji, J. Umeda, K. Kondoh, Rose Bengal-decorated rice husk-derived silica nanoparticles enhanced singlet oxygen generation for antimicrobial photodynamic inactivation, J. Mater. Sci. 58 (6) (2023) 2801–2813.

[96] M.D. Villota-Enríquez, J.E. Rodríguez-Páez, , Bio-silica production from rice husk for environmental remediation: removal of methylene blue from aqueous solutions. Mater. Chem. Phys. 301 (2023) 127671.

[97] T. Islam, J. Liu, G. Shen, T. Ye, C. Peng, Synthesis of chemically modified carbon embedded silica and zeolite from rice husk to adsorb crystal violet dye from aqueous solution, Appl. Ecol. Env. Res. 16 (4) (2018) 3955–3967.

[98] D.V. Thuan, T.T.H. Chu, H.D.T. Thanh, M.V. Le, H.L. Ngo, C.L. Le, H.P. Thi, Adsorption and photodegradation of micropollutant in wastewater by photocatalyst TiO2/rice husk biochar, Environ. Res. (2023) **236**.

[99] S.-G. Yoon, I.-S. Kwak, H.-O. Yoon, J. An, Adsorption characteristics of dimethylated arsenicals on iron oxide–modified rice husk biochar, Toxics 10 (11) (2022) 703.

[100] M.D. Villota-Enríquez, J.E. Rodríguez-Páez, Bio-silica production from rice husk for environmental remediation: removal of methylene blue from aqueous solutions, Mater. Chem. Phys. 301 (2023).

[101] J. Hou, J. Xia, R. Weng, Y. Liu, L. Li, K. Liu, J. Sheng, Y. Song, Mesoporous silicon extracted from rice husk for remediation of different sorts of dyestuffs from simulated textile effluent: kinetic, isotherm, and mechanism study, Biomass-.-. Convers. Biorefin. 13 (18) (2023) 17003–17016.

[102] I.B. Bwatanglang, S.T. Magili, F. Mohammad, H.A. Al-Lohedan, A.A. Soleiman, Biomass-based silica/calcium carbonate nanocomposites for the adsorptive removal of escherichia coli from aqueous suspensions, Separations 10 (3) (2023) 212.
[103] P. Pillai, S. Dharaskar, M. Shah, R. Sultania, Determination of fluoride removal using silica nano adsorbent modified by rice husk from water, Groundw. Sustain. Dev. 11 (2020).
[104] C. Tsamo, G.D. Kidwang, D.C. Dahaina, Removal of rhodamine b from aqueous solution using silica extracted from rice husk, SN Appl. Sci. 2 (2) (2020).
[105] S.S. El-Shafey, S.A. Sayed Ahmed, R.M. Aboelenin, N.A. Fathy, Synthesis of sba-16 mesoporous silica from rice husk ash for removal of rhodamine B cationic dye: effect of hydrothermal treatment time, Desalin. Water Treat. 317 (2024).
[106] W.M. Youssef, M.S. Hagag, A.H. Ali, Synthesis, Characterization and application of composite derived from rice husk ash with aluminium oxide for sorption of uranium, Adsorpt. Sci. Technol. 36 (5-6) (2018) 1274–1293.
[107] G.A. Dakroury, S.F. Abo-Zahra, H.S. Hassan, N.A. Fathy, Utilization of silica–chitosan nanocomposite for removal of 152+ 154Eu radionuclide from aqueous solutions, J. Radioanal. Nucl. Chem. 323 (1) (2020) 439–455.
[108] F. Nie, K. Guan, C. Zou, Z. Xu, Z. Liu, Synthesis of nagnetic rice husk biochar and its application in the adsorption of Ni(II) from aqueous solutions, Biomass-.-. Conv. Bioref. 14 (15) (2024) 18267–18279.
[109] T.H. Pham, T.T.H. Chu, D.K. Nguyen, T.K.O. Le, S.A. Obaid, S.A. Alharbi, J. Kim, M.V. Nguyen, Alginate-modified biochar derived from rice husk waste for improvement uptake performance of lead in wastewater, Chemosphere 307 (2022) 135956.
[110] Y. Mochizuki, J. Bud, J. Liu, N. Tsubouchi, Production of silicone tetrachloride from rice husk by chlorination and performance of mercury adsorption from aqueous solution of the chlorinated residue, ACS Omega 5 (45) (2020) 29110–29120.
[111] S.K. Abbas, Z.M. Hassan, H.H. Mihsen, M.T. Eesa, D.H. Attol, Uptake of nickel(ii) ion by silica-o-phenylenediamine derived from rice husk ash, Silicon 12 (5) (2020) 1103–1110.
[112] N.D. Suzaimi, P.S. Goh, N.A.N.N. Malek, J.W. Lim, A.F. Ismail, Enhancing the performance of porous rice husk silica through branched polyethyleneimine grafting for phosphate adsorption, Arab. J. Chem. 13 (8) (2020) 6682–6695.
[113] M.S. Mahmud, F.D.M. Daud, N. Sariffudin, H.H. Mohd Zaki, N.H. Nordin, N. F. Mohammad, High purity nano-silica from rice husk ash (RHA) via chemical method as additive/stabilizing agent for co2 capture application, Key Eng. Mater. 908 (2022) 373–378.
[114] M. Genovese, A. Schlüter, E. Scionti, F. Piraino, O. Corigliano, P. Fragiacomo, Power-to-hydrogen and Hydrogen-to-X Energy Systems for the Industry of the Future in Europe, Int. J. Hydrog. Energy 48 (44) (2023) 16545–16568.
[115] A. Chapman, K. Itaoka, K. Hirose, F.T. Davidson, K. Nagasawa, A.C. Lloyd, M. E. Webber, Z. Kurban, S. Managi, T. Tamaki, et al., A review of four case studies assessing the potential for hydrogen penetration of the future energy system, Int. J. Hydrog. Energy 44 (13) (2019) 6371–6382.
[116] G.S. Seck, E. Hache, J. Sabathier, F. Guedes, G.A. Reigstad, J. Straus, O. Wolfgang, J.A. Ouassou, M. Askeland, I. Hjorth, et al., Hydrogen and the decarbonization of the energy system in Europe in 2050: a detailed model-based analysis, Renew. Sustain. Energy Rev. 167 (2022) 112779.
[117] N.N. Nguyen, Prospect and challenges of hydrate-based hydrogen storage in the low-carbon future, Energy Fuels 37 (14) (2023) 9771–9789.
[118] Y. Zhu, B. Li, J. Miao, S. Sun, Y. Wang, X. Zhao, B. Chen, C. Wu, Achieving zero co2 emissions from integrated biomass gasification with co2 capture and utilization (IGCCU), Chem. Eng. J. 474 (2023) 145767.
[119] N.N. Nguyen, V.T. La, C.D. Huynh, A.V. Nguyen, Technical and economic perspectives of hydrate-based carbon dioxide capture, Appl. Energy 307 (2021) 118237.
[120] E.D. Sloan, Fundamental principles and applications of natural gas hydrates, Nature 426 (6964) (2003) 353–359.
[121] C.A. Koh, E.D. Sloan, A.K. Sum, D.T. Wu, Fundamentals and Applications of Gas Hydrates, in: J.M. Prausnitz (Ed.), in *Annual Review of Chemical and Biomolecular Engineering*, 2, Annual Reviews: Palo Alto, 2011, pp. 237–257.
[122] N.N. Nguyen, C.V. Nguyen, T.A.H. Nguyen, A.V. Nguyen, Surface science in the research and development of hydrate-based sustainable technologies, ACS Sustain. Chem. Eng. 10 (13) (2022) 4041–4058.
[123] N.N. Nguyen, A.V. Nguyen, The Dual effect of sodium halides on the formation of methane gas hydrate, Fuel 156 (0) (2015) 87–95.
[124] J.S. Yun, J.H. Kim, S.C. Kang, J.S. Im, Mechanism of activated carbon-catalyzed methane decomposition process for the production of hydrogen and high-value carbon, Carbon Lett. 33 (6) (2023) 1799–1809.
[125] R. Zhao, N. Xiao, Y. Liu, W. Zhan, Z. Wu, Study on extraction of silica from rice husk by sol–gel method and its application in catalytic decomposition of methane, Biomass-.-. Convers. Biorefin. 14 (9) (2024) 10067–10083.
[126] A. Farooq, S.-H. Jang, S.H. Lee, S.-C. Jung, G.H. Rhee, B.-H. Jeon, Y.-K. Park, Catalytic steam gasification of food waste using ni-loaded rice husk derived biochar for hydrogen production, Chemosphere 280 (2021) 130671.
[127] F. Guo, K. Peng, S. Liang, X. Jia, X. Jiang, L. Qian, One-step synthesis of biomass activated char supported copper nanoparticles for catalytic cracking of biomass primary Tar, Energy 180 (2019) 584–593.
[128] Q. Dong, H. Li, S. Zhang, X. Li, W. Zhong, Biomass tar cracking and syngas production using rice husk rhar-supported nickel catalysts coupled with microwave heating, RSC Adv. 8 (71) (2018) 40873–40882.
[129] W. Guo, G. Li, Y. Zheng, K. Li, Nano-silica extracted from rice husk and its application in acetic acid steam reforming, RSC Adv. 11 (55) (2021) 34915–34922.
[130] P. Suriya, N. Prasongthum, P. Natewong, T. Wasanapiarnpong, X. Gao, T.S. Zhao, J. Tian, S. Mhadmhan, T.L.M. Hong, P. Reubroycharoen, Hydrogen Production by steam reforming of fusel oil over nickel deposited on pyrolyzed rice husk supports, Energy Rep. 9 (2023) 462–469.
[131] X. Zeng, M. Fang, T. Lv, J. Tian, Z. Xia, J. Cen, Q. Wang, Hydrogen-rich gas production by catalytic steam gasification of rice husk using CeO2-modified Ni-CaO Sorption Bifunctional Catalysts, Chem. Eng. J. 441 (2022) 136023.
[132] P. Qi, Y. Su, L. Yang, J. Wang, M. Jiang, Y. Xiong, Catalytic pyrolysis of rice husk to co-produce hydrogen-rich syngas, phenol-rich bio-oil and nanostructured porous carbon, Energy 298 (2024).
[133] D. Dhinasekaran, R. Raj, A.R. Rajendran, B. Purushothaman, B. Subramanian, A. Prakasarao, G. Singaravelu, Chitosan mediated 5-fluorouracil functionalized silica nanoparticle from rice husk for anticancer activity, Int. J. Biol. Macromol. 156 (2020) 969–980.
[134] S.Y. Chen, J.Y. Jian, H.M. Lin, Functionalization of Rice Husk-derived Mesoporous Silica Nanoparticles For Targeted And Imaging In Cancer Drug Delivery, J. Sci. Food Agric. 104 (4) (2024) 2120–2129.
[135] P. Soundharraj, D. Dhinasekaran, A. Rakkesh Rajendran, A. Prakasarao, S. Ganesan, Investigation on the drug loading efficacy of protoporphyrin functionalized silica precursors (tetraethyl orthosilicate: teos and biomass silica) for enhanced delivery of 5-fluorouracil, ChemistrySelect 8 (20) (2023).
[136] J.L. Andrade, C.A. Moreira, A.G. Oliveira, C.F. de Freitas, M.C. Montanha, A.A. W. Hechenleitner, E.A.G. Pineda, D.M.F. de Oliveira, Rice husk-derived mesoporous silica as a promising platform for chemotherapeutic drug delivery, Waste Biomass-.-. Valoriz. 13 (1) (2022) 241–254.
[137] D. Sarti, R. Einhaus, Silicon Feedstock for the multi-crystalline photovoltaic industry, Sol. Energy Mater. Sol. Cells 72 (1) (2002) 27–40.
[138] M. Tao, Inorganic photovoltaic solar cells: silicon and beyond, Electrochem. Soc. Interface 17 (4) (2008) 30.
[139] G. Bye, B. Ceccaroli, Solar grade silicon: technology status and industrial trends, Sol. Energy Mater. Sol. Cells 130 (2014) 634–646.
[140] F. Farirai, M. Ozonoh, T.C. Aniokete, O. Eterigho-Ikelegbe, M. Mupa, B. Zeyi, M. O. Daramola, Methods of extracting silica and silicon from agricultural waste ashes and application of the produced silicon in solar cells: a mini-review, Int. J. Sustain. Eng. 14 (1) (2021) 57–78.
[141] J.C. Marchal, D.J. Krug Iii, P. McDonnell, K. Sun, R.M. Laine, A low cost, low energy route to solar grade silicon from rice hull ash (RHA), a Sustainable Source, Green. Chem. 17 (7) (2015) 3931–3940.
[142] S.R. Priyan, G.S. Kumar, K. Lalithambigai, M. Shkir, A. Khan, R. Rajendran, G. Arumugam, Microwave-assisted sol-gel synthesis of mesoporous NiO-decorated silica nanostructures utilizing biogenic silica source for supercapacitor applications, J. Alloy. Compd. 976 (2024).
[143] W. Wang, Z. Wang, J. Liu, Y. Peng, X. Yu, W. Wang, Z. Zhang, L. Sun, One-pot facile synthesis of graphene quantum dots from rice husks for fe3+ sensing, Ind. Eng. Chem. Res. 57 (28) (2018) 9144–9150.
[144] Z. Wang, J. Yu, X. Zhang, N. Li, B. Liu, Y. Li, Y. Wang, W. Wang, Y. Li, L. Zhang, et al., Large-scale and controllable synthesis of graphene quantum dots from rice husk biomass: a comprehensive utilization strategy, ACS Appl. Mater. Interfaces 8 (2) (2016) 1434–1439.
[145] Z. Wang, J. Liu, W. Wang, Z. Wei, F. Wang, P. Gong, J. Wang, N. Li, B. Liu, Z. Zhang, et al., Photoluminescent carbon quantum dot grafted silica nanoparticles directly synthesized from rice husk biomass, J. Mater. Chem. B 5 (24) (2017) 4679–4689.
[146] Z. Wei, Z. Wang, W.R.T. Tait, M. Pokhrel, Y. Mao, J. Liu, L. Zhang, W. Wang, L. Sun, Synthesis of green phosphors from highly active amorphous silica derived from rice husks, J. Mater. Sci. 53 (3) (2018) 1824–1832.
[147] J. Alvarez, G. Lopez, M. Amutio, J. Bilbao, M. Olazar, Physical activation of rice husk pyrolysis char for the production of high surface area activated carbons, Ind. Eng. Chem. Res. 54 (29) (2015) 7241–7250.
[148] E. Menya, P.W. Olupot, H. Storz, M. Lubwama, Y. Kiros, Production and performance of activated carbon from rice husks for removal of natural organic matter from water: a review, Chem. Eng. Res. Des. 129 (2018) 271–296.
[149] A.H. Wazir, I.U. Wazir, A.M. Wazir, Preparation and characterization of rice husk based physical activated carbon, Energy Sources, Part A 46 (1) (2024) 4875–4885.
[150] D. Kalderis, S. Bethanis, P. Paraskeva, E. Diamadopoulos, Production of activated carbon from bagasse and rice husk by a single-stage chemical activation method at low retention times, Bioresour. Technol. 99 (15) (2008) 6809–6816.
[151] W.K. Setiawan, K.Y. Chiang, Eco-friendly rice husk pre-treatment for preparing biogenic silica: gluconic acid and citric acid comparative study, Chemosphere 279 (2021).
[152] W.K. Setiawan, K.-Y. Chiang, Facile and green synthesis of disordered mesoporous silica as biogenic filler for mixed-matrix membranes, Mater. Chem. Phys. 307 (2023) 128087.
[153] A.S. Lozano Pérez, J.J. Lozada Castro, C.A. Guerrero Fajardo, Application of microwave energy to biomass: a comprehensive review of microwave-assisted technologies, optimization parameters, and the strengths and weaknesses, J. Manuf. Mater. Process. 8 (3) (2024) 121.
[154] R.V. Kapoore, T.O. Butler, J. Pandhal, S. Vaidyanathan, Microwave-assisted extraction for microalgae: from biofuels to biorefinery, Biology 7 (1) (2018) 18.
[155] G. Cravotto, L. Boffa, S. Mantegna, P. Perego, M. Avogadro, P. Cintas, Improved extraction of vegetable oils under high-intensity ultrasound and/or microwaves, Ultrason. Sonochem. 15 (5) (2008) 898–902.
[156] H.B. Jadhav, I. Raina, P.R. Gogate, U.S. Annapure, F. Casanova, Sonication as a promising technology for the extraction of triacylglycerols from fruit seeds—a review, Food Bioprocess Technol. 16 (8) (2023) 1625–1651.

[157] J. Asomaning, S. Haupt, M. Chae, D.C. Bressler, Recent developments in microwave-assisted thermal conversion of biomass for fuels and chemicals, Renew. Sustain. Energy Rev. 92 (2018) 642–657.
[158] Y. Sheng, S.S. Lam, Y. Wu, S. Ge, J. Wu, L. Cai, Z. Huang, Q.V. Le, C. Sonne, C. Xia, Enzymatic conversion of pretreated lignocellulosic biomass: a review on influence of structural changes of lignin, Bioresour. Technol. Rep. 324 (2021) 124631.
[159] S. Rebello, A.N. Anoopkumar, E.M. Aneesh, R. Sindhu, P. Binod, A. Pandey, Sustainability and life cycle assessments of lignocellulosic and algal pretreatments, Bioresour. Technol. Rep. 301 (2020) 122678.
[160] G. Banerjee, J.S. Scott-Craig, J.D. Walton, Improving enzymes for biomass conversion: a basic research perspective, BioEnergy Res 3 (1) (2010) 82–92.
[161] N.K. Sharma, W.S. Williams, A. Zangvil, Formation and structure of silicon carbide whiskers from rice hulls, J. Am. Ceram. Soc. 67 (11) (1984) 715–720.
[162] N.A.A. Ismail, M.A. Azmi, S. Ahmad, H. Taib, Effect of rice husk firing temperature on synthesis of silica (SiO2), Adv. Mater. Res. 1087 (2015) 470–474.
[163] Z. Chen, H. Chen, Y. Xu, M. Hu, Z. Hu, J. Wang, Z. Pan, Reactor for biomass conversion and waste treatment in supercritical water: a review, Renew. Sustain. Energy Rev. 171 (2023) 113031.
[164] R. Sekifuji, M. Tateda, Study of the feasibility of a rice husk recycling scheme in japan to produce silica fertilizer for rice plants, Sustain. Environ. Res. 29 (1) (2019) 11.